WCAP-10814

WESTINGHOUSE CLASS 3
CUSTOMER DESIGNATED DISTRIBUTION

ANALYSIS OF CAPSULE U FROM THE SOUTH CAROLINA ELECTRIC AND GAS COMPANY VIRGIL C. SUMMER UNIT 1 REACTOR VESSEL RADIATION SURVEILLANCE PROGRAM

R. S. Boggs
A. H. Fero
W.T. Kaiser

June 1985

Work performed under Shop Order No. UCGJ-27302

APPROVED: _____

T. A. Meyer, Manager
Structural Materials and Reliability Technology

Prepared by Westinghouse for the South Carolina Electric and Gas Company

WESTINGHOUSE ELECTRIC CORPORATION
Nuclear Energy Systems
P.O. Box 355
Pittsburgh, Pennsylvania 15230

8455B:1b-061985

PREFACE

This report has been technically reviewed and verified.

	Reviewer	
Sections 1 through 5 and 7	S. E. Yanichko	S E Yanichko
Section 6	S. L. Anderson	S. L. Anderson 6/21/85
Appendix A	W. K. Ma	

LIST OF ILLUSTRATIONS (Cont)

LIST OF TABLES (Cont)

TABLE OF CONTENTS

TABLE OF CONTENTS (Cont)

LIST OF ILLUSTRATIONS

LIST OF ILLUSTRATIONS (Cont)

LIST OF TABLES

LIST OF TABLES (Cont)

SECTION 1
SUMMARY OF RESULTS

The analysis of the reactor vessel material contained in Capsule U, the first surveillance capsule to be removed from the South Carolina Electric and Gas Company V. C. Summer Unit 1 reactor pressure vessel, led to the following conclusions:

- The capsule received an average fast neutron fluence (E > 1.0 MeV) of 6.39×10^{18} n/cm^2.

- Irradiation of the reactor vessel intermediate shell plate A9154-1, to 6.39×10^{18} n/cm, resulted in 30 and 50 ft-lb transition temperature increases of 40°F and 45°F, respectively for specimens oriented parallel to the major working direction (longitudinal orientation) and increases of 30°F and 35°F, respectively for specimens oriented normal to the major working direction (transverse orientation).

- Weld metal irradiated to 6.39×10^{18} n/cm^2 resulted in both a 30 and 50 ft-lb transition temperature increase of 30°F.

- The average upper shelf energy of the plate A9154-1 decreased from 130 to 113 ft-lbs and the limiting weld metal decreased from 104 to 75 ft-lbs. Both materials exhibit a more than adequate shelf level for continued safe plant operation.

- Comparison of the 30 ft-lb transition temperature increases for the V. C. Summer Unit 1 surveillance material with predicted increases using the methods of NRC Regulatory Guide 1.99, Revision 1, shows that the plate material and weld metal transition temperature increase were less than predicted or that the embrittlement was less than predicted.

SECTION 2
INTRODUCTION

This report presents the results of the examination of Capsule U, the first capsule to be removed from the reactor in the continuing surveillance program which monitors the effects of neutron irradiation on the South Carolina Electric and Gas Company V. C. Summer Unit 1 reactor pressure vessel materials under actual operating conditions.

The surveillance program for the South Carolina Electric and Gas Company V. C. Summer Unit 1 reactor pressure vessel materials was designed and recommended by the Westinghouse Electric Corporation. A description of the surveillance program and the preirradiation mechanical properties of the reactor vessel materials are presented by Davidson and Yanichko.[1] The surveillance program was planned to cover the 40-year design life of the reactor pressure vessel and was based on ASTM E-185-73, "Recommended Practice for Surveillance Tests for Nuclear Reactors".[2] Westinghouse Nuclear Energy Systems personnel were contracted to aid in the preparation of procedures for removing the capsule from the reactor and its shipment to the Westinghouse Research and Development Laboratory, where the postirradiation mechanical testing of the Charpy V-notch impact and tensile surveillance specimens was performed.

This report summarizes testing and the postirradiation data obtained from surveillance Capsule U removed from the South Carolina Electric and Gas Company V. C. Summer Unit 1 reactor vessel and discusses the analysis of the data.

SECTION 3
BACKGROUND

The ability of the large steel pressure vessel containing the reactor core and its primary coolant to resist fracture constitutes an important factor in ensuring safety in the nuclear industry. The beltline region of the reactor pressure vessel is the most critical region of the vessel because it is subjected to significant fast neutron bombardment. The overall effects of fast neutron irradiation on the mechanical properties of low alloy ferritic pressure vessel steels such as SA533 Grade B Class 1 plate (base material of the V. C. Summer Unit 1 reactor pressure vessel beltline) are well documented in the literature. Generally, low alloy ferritic materials show an increase in hardness and tensile properties and a decrease in ductility and toughness under certain conditions of irradiation.

A method for performing analyses to guard against fast fracture in reactor pressure vessels has been presented in "Protection Against Non-ductile Failure," Appendix G to Section III of the ASME Boiler and Pressure Vessel Code. The method utilizes fracture mechanics concepts and is based on the reference nil-ductility temperature (RT_{NDT}).

RT_{NDT} is defined as the greater of either the drop weight nil-ductility transition temperature (NDTT per ASTM E-208) or the temperature 60°F less than the 50 ft lb (and 35-mil lateral expansion) temperature as determined from Charpy specimens oriented normal (transverse) to the major working direction of the material. The RT_{NDT} of a given material is used to index that material to a reference stress intensity factor curve (K_{IR} curve) which appears in Appendix G of the ASME Code. The K_{IR} curve is a lower bound of dynamic, crack arrest, and static fracture toughness results obtained from several heats of pressure vessel steel. When a given material is indexed to

the K_{IR} curve, allowable stress intensity factors can be obtained for this material as a function of temperature. Allowable operating limits can then be determined utilizing these allowable stress intensity factors.

RT_{NDT} and, in turn, the operating limits of nuclear power plants can be adjusted to account for the effects of radiation on the reactor vessel material properties. The radiation embrittlement or changes in mechanical properties of a given reactor pressure vessel steel can be monitored by a reactor surveillance program such as the V. C. Summer Unit 1 Reactor Vessel Radiation Surveillance Program,[1] in which a surveillance capsule is periodically removed from the operating nuclear reactor and the encapsulated specimens are tested. The increase in the average Charpy V-notch 30 ft lb temperature (ΔRT_{NDT}) due to irradiation is added to the original RT_{NDT} to adjust the RT_{NDT} for radiation embrittlement. This adjusted RT_{NDT} (RT_{NDT} initial + ΔRT_{NDT}) is used to index the material to the K_{IR} curve and, in turn, to set operating limits for the nuclear power plant which take into account the effects of irradiation on the reactor vessel materials.

SECTION 4
DESCRIPTION OF PROGRAM

Six surveillance capsules for monitoring the effects of neutron exposure on the V. C. Summer Unit 1 reactor pressure vessel core region material were inserted in the reactor vessel prior to initial plant startup. The capsules were positioned in the reactor vessel between the neutron shielding pads and the vessel wall at locations shown in figure 4-1. The vertical center of the capsules is opposite the vertical center of the core.

Capsule U was removed after 1.12 effective full power years of plant operation. This capsule contained Charpy V-notch impact, tensile, and CT specimens (figure 4-2) from the intermediate shell plate A9154-1 and submerged arc weld metal representative of the beltline weld seams of the reactor vessel and Charpy V-notch specimens from weld heat-affected zone (HAZ) material. All heat-affected zone specimens were obtained from within the HAZ of plate A9154-1 of the representative weld.

The chemistry and heat treatment of the surveillance material are presented in table 4-1 and table 4-2, respectively. The chemical analyses reported in table 4-1 were obtained from unirradiated material used in the surveillance program. In addition, a chemical analysis was performed on an irradiated Charpy specimen from the weld metal and is reported in table 4-1.

All test specimens were machined from the 1/4 thickness location of the plate. Test specimens represent material taken at least one plate thickness from the quenched end of the plate. Base metal Charpy V-notch impact specimens were oriented with the longitudinal axis of the specimen parallel to the major working direction of the plate (longitudinal orientation). Charpy V-notch and tensile specimens from the weld metal were oriented with the

longitudinal axis of the specimens transverse to the welding direction. The CT specimens in Capsule U were machined such that the simulated crack in the specimen would propagate normal and parallel to the major working direction for the plate specimen and parallel to the weld direction.

Capsule U contained dosimeter wires of pure iron, copper, nickel, and aluminum-cobalt (cadmium-shielded and unshielded). In addition, cadmium-shielded dosimeters of Neptunium (Np^{237}) and Uranium (U^{238}) were contained in the capsule.

Thermal monitors made from two low-melting eutectic alloys and sealed in Pyrex tubes were included in the capsule and were located as shown in Figure 4-2. The two eutectic alloys and their melting points are:

2.5% Ag, 97.5% Pb	Melting Point 579°F (304°C)
1.75% Ag, 0.75% Sn, 97.5% Pb	Melting Point 590°F (310°C)

The arrangement of the various mechanical test specimens, dosimeters and thermal monitors contained in Capsule U are shown in Figure 4-2.

TABLE 4-1

CHEMICAL COMPOSITION OF
THE V. C. SUMMER UNIT 1 REACTOR VESSEL
SURVEILLANCE MATERIALS

Element	Plate A9154-1 Lukens Steel Co. Analysis	Weld Metal[c] Lukens Steel Co. Analysis
C	0.22	0.085
S	0.015	0.012/0.007[b]
N_2	0.0076	0.015
Co	0.010	0.016/0.01[b]
Cu	0.10	0.05/0.04[b]
Si	0.24	0.48/0.42[b]
Mo	0.49	0.49/0.46[b]
Ni	0.51	0.91/0.95[b]
Mn	1.30	1.32/1.50[b]
Cr	0.08	0.14/0.12[b]
V	0.001[a]	0.005
P	0.009	0.013/0.009[b]
Sn	0.007	0.0047
Al	0.024	0.007/0.03[b]
B	0.0004	0.0005
Ti	0.0002	0.001
Pb	< 0.005	0.0206
Zr	0.001	0.001
As	0.006	0.006
W	< 0.01	0.01

[a] Westinghouse Analysis
[b] Analysis performed on irradiated weld specimen CW14.
[c] Surveillance weld was made of the same RACO INMM wire Heat #4P4784 as the beltline welds of the reactor vessel.

TABLE 4-2

HEAT TREATMENT OF THE V. C. SUMMER UNIT 1
REACTOR VESSEL SURVEILLANCE MATERIALS

Material	Temperature (°F)	Time (hr)	Coolant
Lower Shell Plate A9154-1	1550°/1650°	1/2 hr/in., min	Water quenched
	1225° + 25°	1/2 hr/in., min	Air cooled
	1150° ∓ 25°	43	Furnace cooled to 600°F
Weldment	1150° ± 25°	12	Furnace cooled

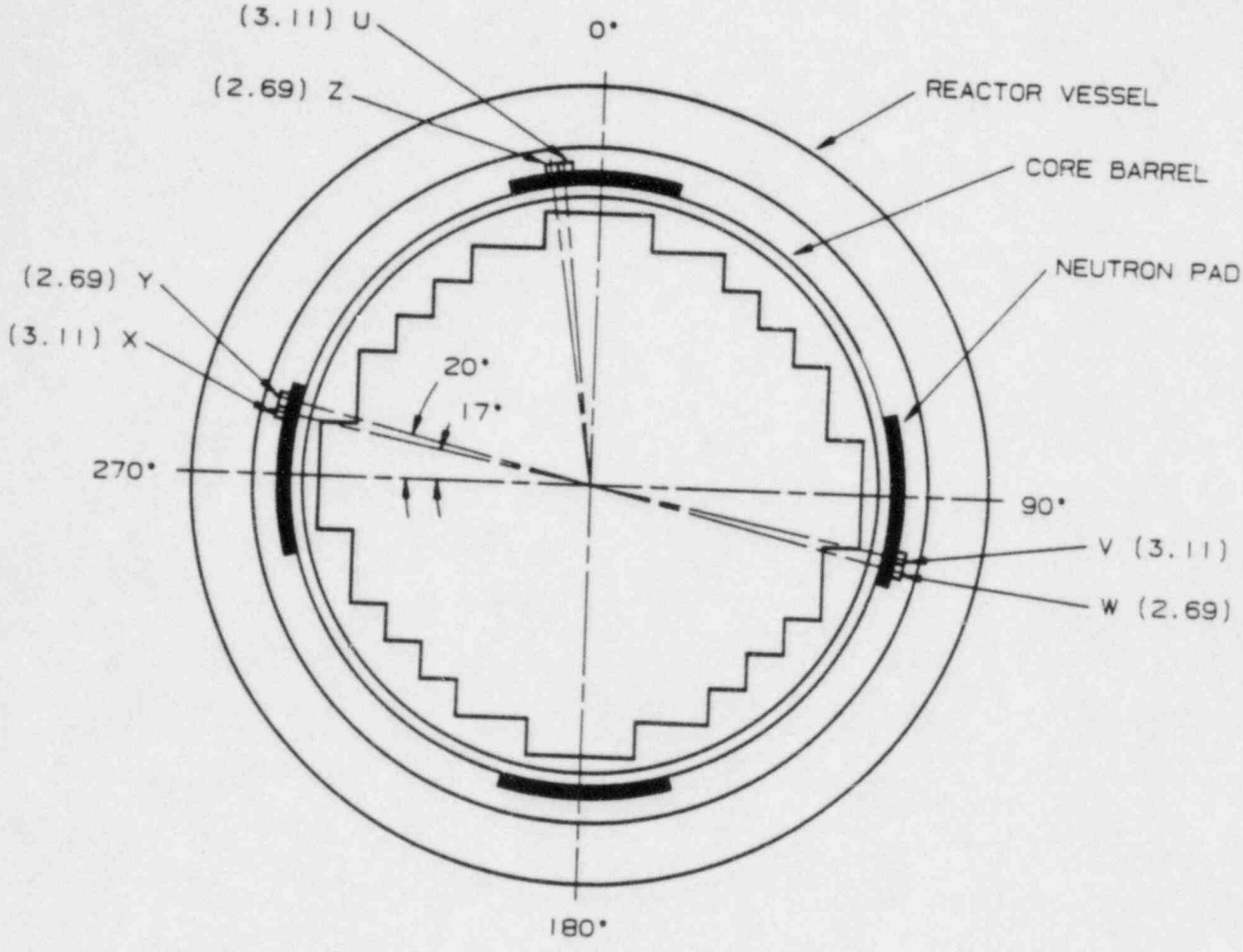

Figure 4-1 Arrangement of Surveillance Capsules in the V.C.Summer Unit 1 Reactor Vessel (Updated Lead Factors for the Capsules Shown in Parentheses.)

SPECIMEN NUMBERING CODE:

CT - PLATE A9154-1 (TRANSVERSE ORIENTATION)
CL - PLATE A9154-1 (LONGITUDINAL ORIENTATION)
CW - CORE REGION WELD METAL
CH - HEAT-AFFECTED-ZONE METAL

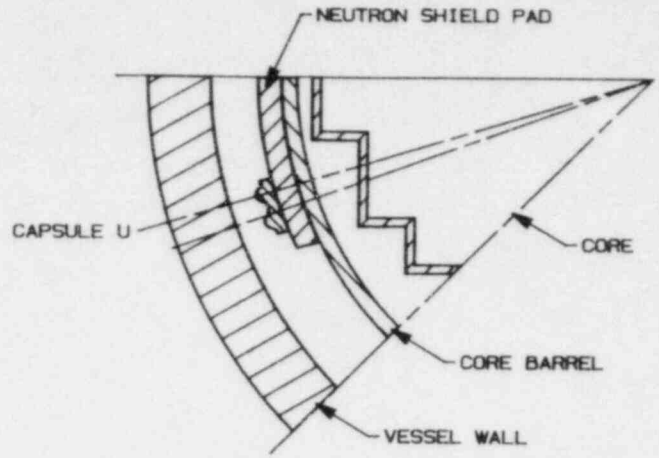

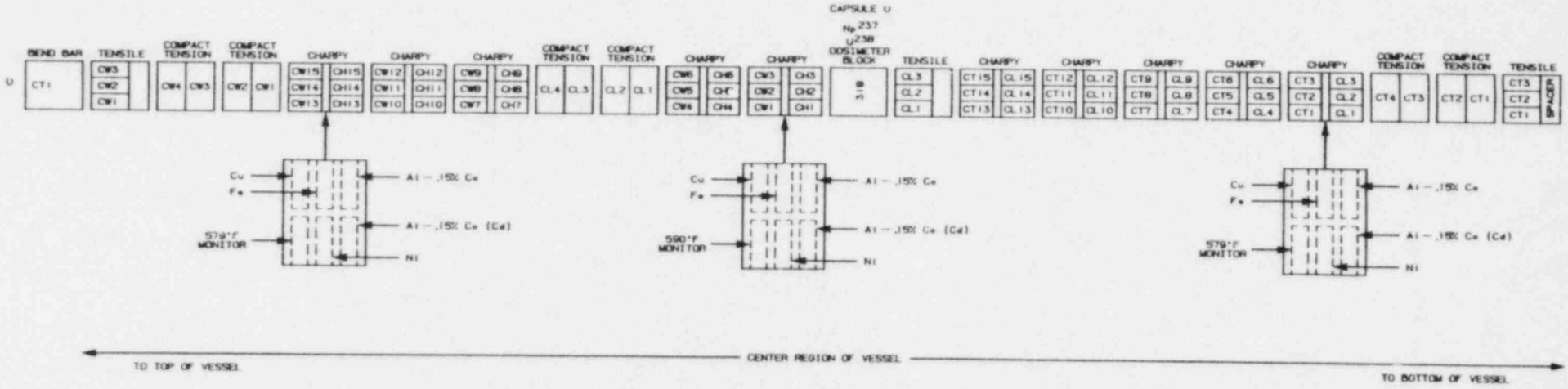

Figure 4-2.
Capsule U Diagram Showing Location of Specimens, Thermal Monitors, and Dosimeters

SECTION 5
TESTING OF SPECIMENS FROM CAPSULE U

5-1. OVERVIEW

The postirradiation mechanical testing of the Charpy V-notch and tensile specimens was performed at the Westinghouse Research and Development Laboratory with consultation by Westinghouse Nuclear Energy Systems personnel. Testing was performed in accordance with 10CFR50, Appendices G and H, ASTM Specification E185-82 and Westinghouse Procedure MHL 8402, Revision 0 as modified by RMF Procedures 8102 and 8103. The mechanical test data was documented in an R&D report by Lott and Shogan.[3]

Upon receipt of the capsule at the laboratory, the specimens and spacer blocks were carefully removed, inspected for identification number, and checked against the master list in WCAP-9234.[1] No discrepancies were found.

Examination of the two low-melting 304°C (579°F) and 310°C (590°F) eutectic alloys indicated no melting of either type of thermal monitor. Based on this examination, the maximum temperature to which the test specimens were exposed was less than 304°C (579°F).

The Charpy impact tests were performed per ASTM Specification E23-82 and RMF Procedure 8103 on a Tinius-Olsen Model 74, 358J machine. The tup (striker) of the Charpy machine is instrumented with an Effects Technology model 500 instrumentation system. With this system, load-time and energy-time signals can be recorded in addition to the standard measurement of Charpy energy (E_D). From the load-time curve, the load of general yielding (P_{GY}), the time to general yielding (t_{GY}), the maximum load (P_M), and the time to maximum load (t_M) can be determined. Under some test conditions, a sharp

drop in load indicative of fast fracture was observed. The load at which fast fracture was initiated is identified as the fast fracture load (P_F), and the load at which fast fracture terminated is identified as the arrest load (P_A).

The energy at maximum load (E_M) was determined by comparing the energy-time record and the load-time record. The energy at maximum load is approximately equivalent to the energy required to initiate a crack in the specimen. Therefore, the propagation energy for the crack (E_p) is the difference between the total energy to fracture (E_D) and the energy at maximum load.

The yield stress (σy) is calculated from the three point bend formula. The flow stress is calculated from the average of the yield and maximum loads, also using the three point bend formula.

Percentage shear was determined from postfracture photographs using the ratio-of-areas methods in compliance with ASTM Specification A370-77. The lateral expansion was measured using a dial gage rig similar to that shown in the same specification.

Tension tests were performed on a 20,000-pound Instron, split-console test machine (Model 1115) per ASTM Specifications E8-83 and E21-79, and RMF Procedure 8102. All pull rods, grips, and pins were made of Inconel 718 hardened to Rc45. The upper pull rod was connected through a universal joint to improve axiality of loading. The tests were conducted at a constant crosshead speed of 0.05 inch per minute throughout the test.

Deflection measurements were made with a linear variable displacement transducer (LVDT) extensometer. The extensometer knife edges were spring-loaded to the specimen and operated through specimen failure. The extensometer gage length is 1.00 inch. The extensometer is rated as Class B-2 per ASTM E83-67.

Elevated test temperatures were obtained with a three-zone electric resistance split-tube furnace with a 9-inch hot zone. All tests were conducted in air.

Because of the difficulty in remotely attaching a thermocouple directly to the specimen, the following procedure was used to monitor specimen temperature. Chromel-alumel thermocouples were inserted in shallow holes in the center and each end of the gage section of a dummy specimen and in each grip. In test configuration, with a slight load on the specimen, a plot of specimen temperature versus upper and lower grip and controller temperatures was developed over the range room temperature to 550°F (288°C). The upper grip was used to control the furnace temperature. During the actual testing the grip temperatures were used to obtain desired specimen temperatures. Experiments indicated that this method is accurate to plus or minus 2°F.

The yield load, ultimate load, fracture load, total elongation, and uniform elongation were determined directly from the load-extension curve. The yield strength, ultimate strength, and fracture strength were calculated using the original cross-sectional area. The final diameter and final gage length were determined from postfracture photographs. The fracture area used to calculate the fracture stress (true stress at fracture) and percent reduction in area was computed using the final diameter measurement.

5.2. CHARPY V-NOTCH IMPACT TEST RESULTS

The results of Charpy V-notch impact tests performed on the various materials contained in Capsule U irradiated at 6.39×10^{18} n/cm^2 are presented in Tables 5-1 through 5-8 and Figures 5-1 through 5-4. The transition temperature increases and upper shelf energy decreases for the Capsule U material are summarized in Table 5-9.

Irradiation of vessel intermediate shell plate A9154-1 material (longitudinal orientation) specimens to 6.39×10^{18} n/cm^2 (Figure 5-1) resulted in both 30 and 50 ft-lb transition temperature increases of 40°F and 45°F, respectively, and an upper shelf energy decrease of 2 ft-lb.

Irradiation of vessel intermediate shell plate A9154-1 material (transverse orientation) specimens to 6.39×10^{18} m/cm^2 (Figure 5-2) resulted in both 30 and 50 ft-lb transition temperature increases of 30°F and 35°F respectively. The irradiated upper shelf energy experienced no decrease as compared to the unirradiated data.

Weld metal irradiated to 6.39 x 10^{18} n/cm^2 (Figure 5-3) resulted in both 30 and 50 ft-lb transition temperature increases of 30°F and an upper shelf energy decrease of 4 ft-lb.

Weld HAZ metal irradiated to 6.39 x 10^{18} n/cm^2 (Figure 5-4) resulted in both 30 and 50 ft-lb transition temperature increases of 30°F and 35°F, respectively, and an upper shelf energy decrease of 15 ft-lb.

The fracture appearance of each irradiated Charpy specimen from the various materials is shown in Figures 5-5 through 5-8 and show an increasing ductile or tougher appearance with increasing test temperature.

Figure 5-9 shows a comparison of the 30 ft-lb transition temperature increases for the various V. C. Summer Unit 1 surveillance materials with predicted increases using the methods of NRC Regulatory Guide 1.99, Revision 1.[4] This comparison shows that the transition temperature increase resulting from irradiation to 6.39 x 10^{18} n/cm^2 is less than predicted by the Guide for plate A9154-1 (longitudinal and transverse orientation). The weld metal transition temperature increase resulting from 6.39 x 10^{18} n/cm^2 is also less than the Guide prediction.

5-3. TENSION TEST RESULTS

The results of tension tests performed on plate A9154-1 (longitudinal and transverse orientation) and weld metal irradiated to 6.39 x 10^{18} n/cm^2 are shown in Table 5-10 and Figures 5-10, 5-11 and 5-12, respectively. These results shown that irradiation produced no increase in 0.2 percent yield strength for plate A9154-1 and approximately a 2 ksi increase for the weld metal. Fractured tension specimens for each of the materials are shown in Figures 5-13, 5-14 and 5-15. A typical stress-strain curve for the tension specimens is shown in Figure 5-16.

5-4. COMPACT TENSION TEST

Per the Surveillance Capsule Testing Contract with South Carolina Electric and Gas, 1/2T compact tension (CT) specimen will not be tested. CT specimen will be stored at the Hot Cell at the Westinghouse R&D Center.

TABLE 5-1

CHARPY V-NOTCH IMPACT DATA FOR THE V. C. SUMMER UNIT 1
INTERMEDIATE SHELL PLATE A9154-1 (LONGITUDINAL)
IRRADIATED AT 550°F, FLUENCE 6.39 x 10^{18} n/cm^2 (E > 1 MeV)

Sample No.	Temperature °F (°C)	Impact Energy ft-lbs (Joules)	Lateral Expansion mils (mm)	% Shear
CL11	-25 (-32)	7.0 (9.5)	3.5 (0.09)	11
CL1	0 (-18)	16.0 (21.5)	11.0 (0.28)	16
CL5	25 (-4)	43.0 (58.5)	32.0 (0.81)	14
CL2	25 (-4)	21.0 (28.5)	19.0 (0.48)	12
CL15	25 (-4)	38.0 (51.5)	28.0 (0.71)	18
CL9	50 (10)	42.0 (57.0)	31.5 (0.80)	20
CL7	50 (10)	70.0 (95.0)	51.0 (1.30)	32
CL8	75 (24)	84.0 (114.0)	56.5 (1.44)	38
CL13	100 (38)	60.0 (81.5)	42.0 (1.07)	37
CL4	100 (38)	77.0 (104.5)	55.0 (1.40)	44
CL14	150 (66)	109.0 (148.0)	77.0 (1.96)	62
CL3	200 (93)	118.0 (160.0)	80.0 (2.03)	97
CL12	250 (121)	126.0 (171.0)	90.0 (2.29)	100
CL10	300 (149)	135.0 (183.0)	86.0 (2.18)	100
CL6	350 (177)	132.0 (179.0)	84.0 (2.13)	100

TABLE 5-2

CHARPY V-NOTCH IMPACT DATA FOR THE V.C. SUMMER UNIT 1
INTERMEDIATE SHELL PLATE A9154-1 (TRANSVERSE)
IRRADIATED AT 550°F, FLUENCE 6.39 x 10^{18} n/cm^2 (E > 1 MeV)

Sample No.	Temperature °F (°C)	Impact Energy ft-lbs (Joules)	Lateral Expansion mils (mm)	% Shear
CT6	-50 (-46)	5.0 (7.0)	2.5 (0.06)	0
CT10	0 (-18)	23.0 (31.0)	15.5 (0.39)	2
CT7	0 (-18)	15.0 (20.5)	12.5 (0.32)	1
CT4	25 (-4)	24.0 (32.5)	19.0 (0.48)	5
CT12	25 (-4)	23.0 (31.0)	20.5 (0.52)	4
CT3	50 (10)	32.0 (43.5)	24.5 (0.62)	10
CT1	50 (10)	17.0 (23.0)	19.0 (0.48)	8
CT14	75 (24)	69.0 (93.5)	52.5 (1.33)	86
CT2	76 (24)	36.0 (49.0)	31.5 (0.80)	86
CT15	100 (38)	49.0 (66.5)	42.5 (1.08)	95
CT13	150 (66)	61.0 (82.5)	52.0 (1.32)	97
CT9	200 (93)	70.0 (95.0)	62.5 (1.59)	100
CT11	300 (149)	76.0 (103.0)	65.0 (1.65)	100
CT8	350 (177)	80.0 (108.5)	73.0 (1.85)	100

TABLE 5-3

CHARPY V-NOTCH IMPACT DATA FOR THE V.C. SUMMER UNIT 1
PRESSURE VESSEL WELD METAL IRRADIATED AT 550°F,
FLUENCE 6.39 x 10^{18} n/cm^2 (E > 1 MeV)

Sample No.	Temperature °F (°C)	Impact Energy ft-lbs (Joules)	Lateral Expansion mils (mm)	% Shear
CW9	-100 (-73)	7.0 (9.5)	7.0 (0.18)	2
CW2	-60 (-51)	24.0 (32.5)	18.0 (0.46)	16
CW7	-40 (-40)	26.0 (35.5)	20.5 (0.52)	25
CW13	-25 (-32)	22.0 (30.0)	23.0 (0.58)	37
CW3	-25 (-32)	38.0 (51.5)	26.0 (0.66)	26
CW14	-10 (-23)	43.0 (58.5)	33.0 (0.84)	37
CW12	0 (-18)	44.0 (59.5)	35.0 (0.89)	42
CW6	0 (-18)	49.0 (66.5)	37.0 (0.94)	54
CW4	25 (-4)	54.0 (73.0)	44.0 (1.12)	58
CW15	50 (10)	58.0 (78.5)	51.5 (1.31)	65
CW11	75 (24)	84.0 (114.0)	72.0 (1.83)	100
CW10	100 (38)	86.0 (116.5)	70.0 (1.78)	100
CW5	150 (66)	86.0 (116.5)	71.0 (1.80)	100
CW1	200 (93)	86.0 (116.5)	57.0 (1.45)	100
CW8	300 (149)	92.0 (124.5)	60.5 (1.54)	100

TABLE 5-4

CHARPY V-NOTCH IMPACT DATA FOR THE V.C. SUMMER UNIT 1
PRESSURE VESSEL WELD HEAT AFFECTED ZONE METAL
IRRADIATED AT 550°F, FLUENCE 6.39 x 10^{18} n/cm^2 (E > 1 MeV)

Sample No.	Temperature °F (°C)	Impact Energy ft-lbs (Joules)	Lateral Expansion mils (mm)	% Shear
CH2	-100 (-73)	18.0 (24.5)	11.0 (0.28)	11
CH13	-60 (-51)	32.0 (43.5)	26.5 (0.67)	18
CH14	-40 (-40)	37.0 (50.0)	22.5 (0.57)	20
CH3	-40 (-40)	38.0 (51.5)	27.0 (0.69)	26
CH7	-25 (-32)	53.0 (72.0)	40.0 (1.02)	30
CH11	0 (-18)	79.0 (107.0)	49.5 (1.26)	60
CH15	25 (-4)	71.0 (96.5)	56.5 (1.44)	57
CH8	25 (-4)	92.0 (124.5)	60.5 (1.54)	79
CH9	50 (10)	95.0 (129.0)	70.0 (1.78)	100
CH6	50 (10)	118.0 (160.0)	69.5 (1.77)	100
CH4	75 (24)	124.0 (168.0)	80.5 (2.04)	100
CH12	100 (38)	99.0 (134.0)	66.5 (1.69)	100
CH1	150 (66)	125.0 (169.5)	81.5 (2.07)	100
CH10	200 (93)	148.0 (200.5)	84.0 (2.13)	100
CH5	300 (149)	138.0 (187.0)	77.0 (1.96)	100

TABLE 5-5

INSTRUMENTED CHARPY IMPACT TEST RESULTS FOR V. C. SUMMER UNIT 1

INTERMEDIATE SHELL PLATE A9154-1 (LONGITUDINAL ORIENTATION)

Sample No.	Test Temp. (°C)	Charpy Energy (Joules)	Normalized Energies: Charpy Ed/A (kJ/m^2)	Maximum Em/A (kJ/m^2)	Prop Ep/A (kJ/m^2)	Yield Load (N)	Time to Yield (µSec)	Maximum Load (N)	Time to Maximum (µSec)	Fracture Load (N)	Arrest Load (N)	Yield Stress (MPa)	Flow Stress (MPa)
CL11	-32	9.5	119	58	60	15100	90	15500	100	15200	300	779	788
CL1	-18	21.5	271	221	50	15000	105	17400	270	17400	0	770	843
CL2	-4	28.5	356	223	133	15100	95	17200	270	17200	800	776	831
CL15	-4	51.5	644	546	98	15000	95	19100	270	19100	100	769	881
CL5	-4	58.5	729	634	94	14700	100	19200	570	19200	200	759	874
CL9	10	57.0	712	559	153	13100	90	17900	665	17900	0	675	798
CL7	10	95.0	1186	643	543	14100	90	19200	625	16700	2200	723	857
CL8	24	114.0	1424	639	785	13100	85	18300	675	16200	6700	675	808
CL13	38	81.5	1017	685	331	12900	95	17800	695	17300	5500	663	789
CL4	38	104.5	1305	636	669	13200	100	18500	775	15800	5200	680	817
CL14	66	148.0	1847	700	1148	13000	95	18000	695			670	799
CL3	93	160.0	2000	584	1416	12800	95	17700	775			660	784
CL12	121	171.0	2135	619	1516	10300	85	16600	765			528	690
CL10	149	183.0	2288	581	1707	9100	130	16100	780			469	649
CL6	177	179.0	2237	604	1633	11200	90	16500	725			577	713

TABLE 5-6

INSTRUMENTED CHARPY IMPACT TEST RESULTS

FOR V. C. SUMMER UNIT 1

INTERMEDIATE SHELL PLATE A9154-1 (TRANSVERSE ORIENTATION)

Sample No.	Test Temp. (°C)	Charpy Energy (Joules)	Normalized Energies: Charpy Ed/A (kJ/m^2)	Maximum Em/A (kJ/m^2)	Prop Ep/A (kJ/m^2)	Yield Load (N)	Time to Yield (µSec)	Maximum Load (N)	Time to Maximum (µSec)	Fracture Load (N)	Arrest Load (N)	Yield Stress (MPa)	Flow Stress (MPa)
CT6	-46	7.0	85	38	47	13000	80	13700	85	13400	0	668	686
CT7	-18	20.5	254	147	108	12900	85	15000	220	14700	0	664	717
CT10	-18	31.0	390	308	82	14800	100	18200	355	17900	0	763	848
CT12	-4	31.0	390	280	109	14500	100	17400	335	17400	700	748	822
CT4	-4	32.5	407	307	100	14300	90	17700	355	17000	500	737	824
CT1	10	23.0	288	111	177	13800	85	15200	160	15200	2600	711	746
CT3	10	43.5	542	361	181	13200	90	17000	435	17000	0	677	775
CT14	24	93.5	1169	462	708	13000	90	17500	530	16300	8900	668	785
CT2	24	49.0	610	278	332	13500	85	17100	335	16800	6700	692	787
CT15	38	66.5	830	507	323	11900	90	16400	620	15600	6700	613	728
CT13	66	82.5	1034	429	605	12700	100	17000	520			652	763
CT9	93	95.0	1186	384	802	12600	95	16300	470			647	743
CT11	149	103.0	1288	434	854	10000	50	16300	530			512	676
CT8	177	108.5	1356	407	949	8400	65	14900	560			432	599

TABLE 5-7

INSTRUMENTED CHARPY IMPACT TEST RESULTS

FOR V. C. SUMMER UNIT 1 WELD METAL

Sample No.	Test Temp. (°C)	Charpy Energy (Joules)	Normalized Energies: Charpy Ed/A (kJ/m^2)	Maximum Em/A (kJ/m^2)	Prop Ep/A (kJ/m^2)	Yield Load (N)	Time to Yield (μSec)	Maximum Load (N)	Time to Maximum (μSec)	Fracture Load (N)	Arrest Load (N)	Yield Stress (MPa)	Flow Stress (MPa)
CW9	-73	9.5	119	83	36	16300	100	17300	125	17000	400	841	865
CW2	-51	32.5	407	328	79	15800	95	19000	355	18600	0	815	897
CW7	-40	35.5	441	335	106	15400	90	19100	360	18700	1500	793	887
CW13	-32	30.0	373	235	138	15500	105	17800	280	17900	2300	800	858
CW3	-32	51.5	644	387	257	15100	110	18800	435	18800	300	778	874
CW14	-23	58.5	729	393	336	12900	70	16900	475	16700	2600	664	766
CW12	-18	59.5	746	464	281	14100	85	18700	500	17800	3600	726	843
CW6	-18	66.5	830	482	348	15100	95	19100	510	18500	5900	779	880
CW4	-4	73.0	915	443	472	13100	85	17700	510	16800	8200	675	792
CW15	10	78.5	983	510	473	13600	90	18000	570	17400	11100	698	812
CW11	24	114.0	1424	513	911	12900	80	18200	560			664	800
CW10	38	116.5	1458	543	915	13700	90	18300	595			705	824
CW5	66	116.5	1458	533	925	13300	90	17800	595			687	803
CW1	93	116.5	1458	563	894	12900	95	17400	650			662	778
CW8	149	124.5	1559	561	998	12600	130	16800	695			648	755

TABLE 5-8

INSTRUMENTED CHARPY IMPACT TEST RESULTS

FOR V. C. SUMMER UNIT 1 WELD HEAT AFFECTED ZONE METAL

Sample No.	Test Temp. (°C)	Charpy Energy (Joules)	Normalized Energies: Charpy Ed/A (kJ/m^2)	Maximum Em/A (kJ/m^2)	Prop Ep/A (kJ/m^2)	Yield Load (N)	Time to Yield (µSec)	Maximum Load (N)	Time to Maximum (µSec)	Fracture Load (N)	Arrest Load (N)	Yield Stress (MPa)	Flow Stress (MPa)
CH2	-73	24.5	305	267	38	17600	110	19800	295	19800	200	906	964
CH13	-51	43.5	542	401	141	16900	100	20100	410	20100	1400	872	954
CH14	-40	50.0	627	490	137	16800	100	20200	495	20100	1200	862	951
CH3	-40	51.5	644	493	151	15700	95	19800	505	18900	200	808	914
CH7	-32	72.0	898	579	320	13800	90	18500	650	16700	5200	711	833
CH11	-18	107.0	1339	604	735	16200	90	19800	605	18200	10900	833	925
CH15	-4	96.5	1203	530	674	12800	90	18000	600	15400	5900	660	794
CH8	-4	124.5	1559	584	976	15100	95	19000	610			776	878
CH9	10	129.0	1610	605	1005	13900	95	18800	650			715	842
CH6	10	160.0	2000	598	1402	13300	85	18200	665			687	811
CH4	24	168.0	2102	721	1381	13100	95	18100	805			674	803
CH12	38	134.0	1678	598	1079	13300	90	18000	675			683	804
CH1	66	169.5	2118	712	1406	13300	90	18700	775			685	822
CH10	93	200.5	2508	606	1903	13100	105	17900	695			673	798
CH5	149	187.0	2339	625	1713	11800	95	17200	740			605	746

TABLE 5-9

EFFECT OF 550°F IRRADIATION AT 6.39 x 10^{18} n/cm^2 (E > 1 MeV)

ON THE NOTCH TOUGHNESS PROPERTIES OF THE

V. C. SUMMER UNIT 1 REACTOR VESSEL MATERIALS

Material	Average 30 ft-lb Temp (°F)			Average 35 mil Lateral Expansion Temp (°F)			Average 50 ft-lb Temp (°F)			Average Energy Absorption at Full Shear (ft-lb)		
	Unirradiated	Irradiated	ΔT	Unirradiated	Irradiated	ΔT	Unirradiated	Irradiated	ΔT	Unirradiated	Irradiated	Δ(ft-lb)
Plate A9154-1 (Longitudinal)	-20	20	40	0	40	40	0	45	45	133	131	2
Plate A9154-1 (Transverse)	25	55	30	55	75	20	70	105	35	75	75	0
Weld Metal	-55	-25	30	-30	0	30	-15	15	30	91	87	4
HAZ Metal	-85	-55	30	-55	-25	30	-65	-30	35	136	121	15

TABLE 5-10

TENSILE PROPERTIES FOR V. C. SUMMER UNIT 1

REACTOR VESSEL MATERIAL IRRADIATED TO 6.39×10^{18} n/cm^2

Sample No.	Material	Test Temp. (°F)	2% Yield Strength (ksi)	Ultimate Strength (ksi)	Fracture Load (kip)	Fracture Stress (ksi)	Fracture Strength (ksi)	Uniform Elongation (%)	Total Elongation (%)	Reduction in Area (%)
CL2	LONG (A9154-1)	100	64.2	88.4	2.80	179.3	57.0	11.0	26.6	68
CL1	LONG (A9154-1)	250	63.2	86.8	2.80	165.0	57.0	10.5	23.4	65
CL3	LONG (A9154-1)	550	62.1	89.6	3.10	160.1	63.2	10.5	22.7	61
CT1	TRANS (A9154-1)	74	64.2	91.7	3.40	146.3	69.3	11.7	23.3	53
CT1	TRANS (A9154-1)	200	59.6	84.3	3.00	159.0	61.1	10.7	22.8	62
CT2	TRANS (A9154-1)	550	56.0	87.6	3.30	168.3	67.2	10.5	20.3	60
CW2	WELD Metal	0	72.6	97.8	3.30	205.5	67.2	12.3	24.8	67
CW3	WELD Metal	74	72.3	92.5	3.10	185.2	63.2	12.3	24.0	66
CW1	WELD Metal	550	66.1	88.4	3.34	128.4	68.0	9.3	15.5	47*

*Specimen CW1 broke at the extensometer knife edge. Ductility values may be in error. (Figure 5-12)

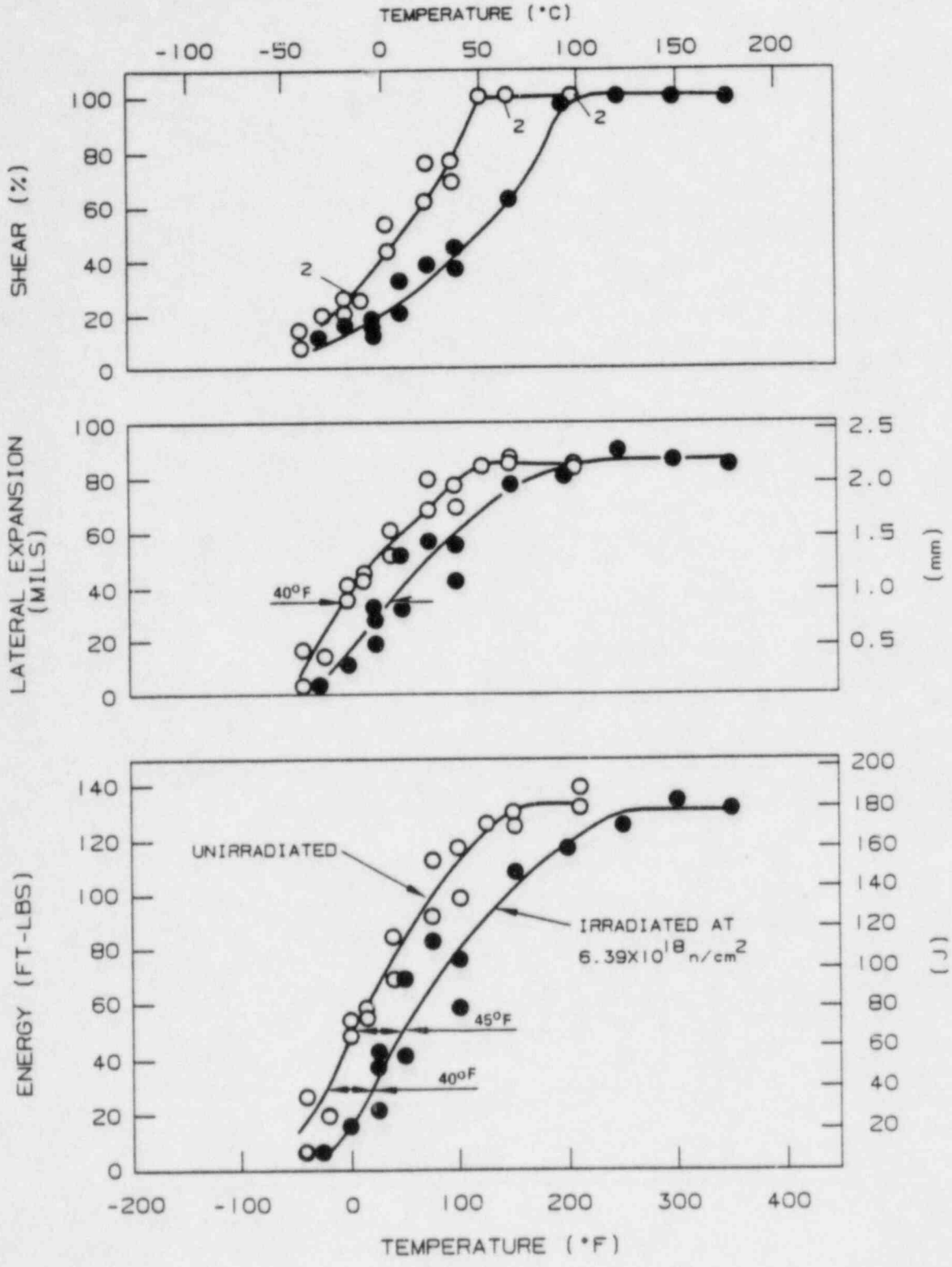

Figure 5-1 Irradiated Charpy V-Notch Impact Properties for V.C.Summer Unit 1 Reactor Vessel Intermediate Shell Plate A9154-1 (Longitudinal Orientation)

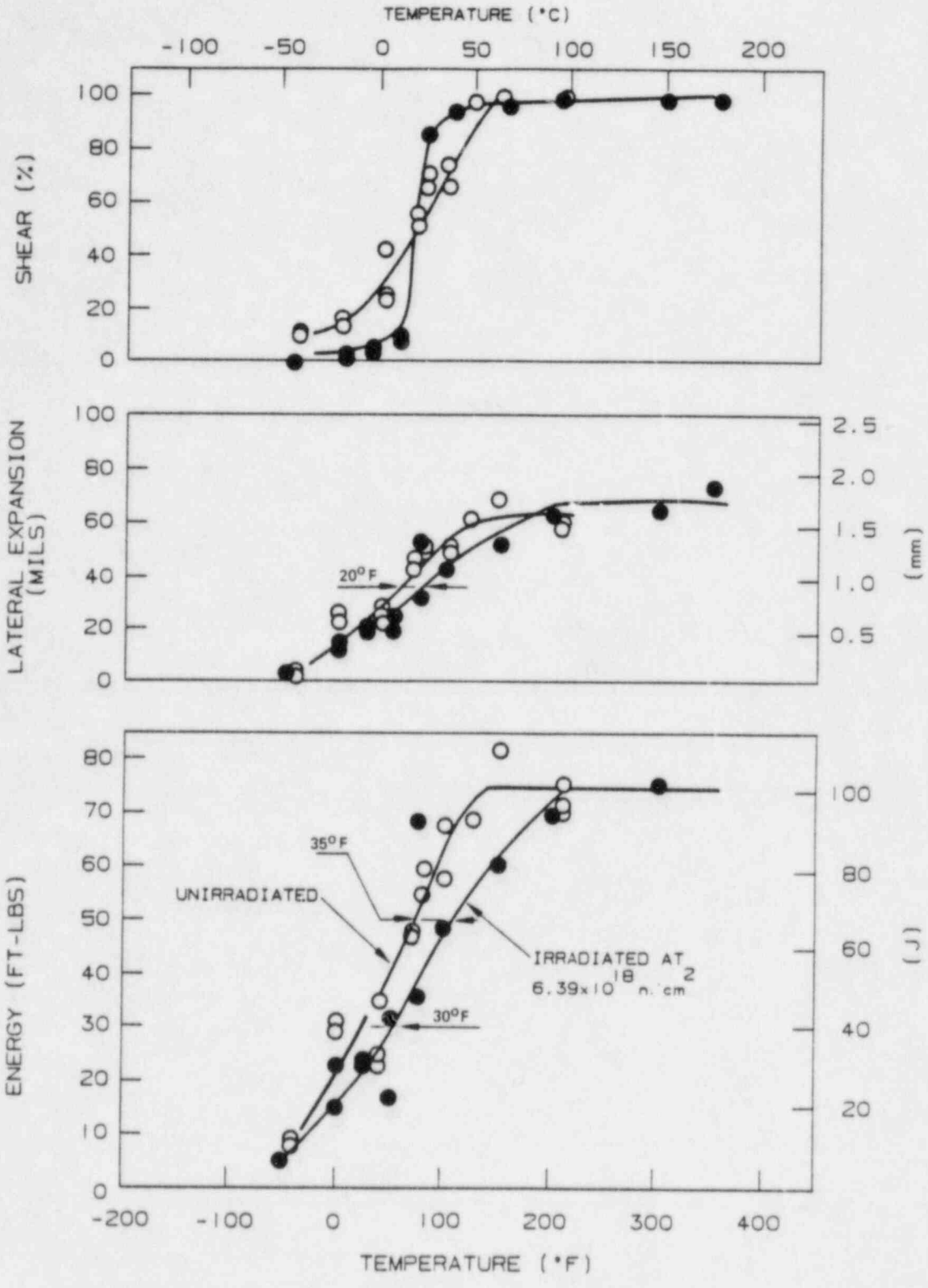

Figure 5-2 Irradiated Charpy V-Notch Impact Properties for V.C.Summer Unit 1 Reactor Pressure Vessel Intermediate Shell Plate A9154-1 (Transverse Orientation)

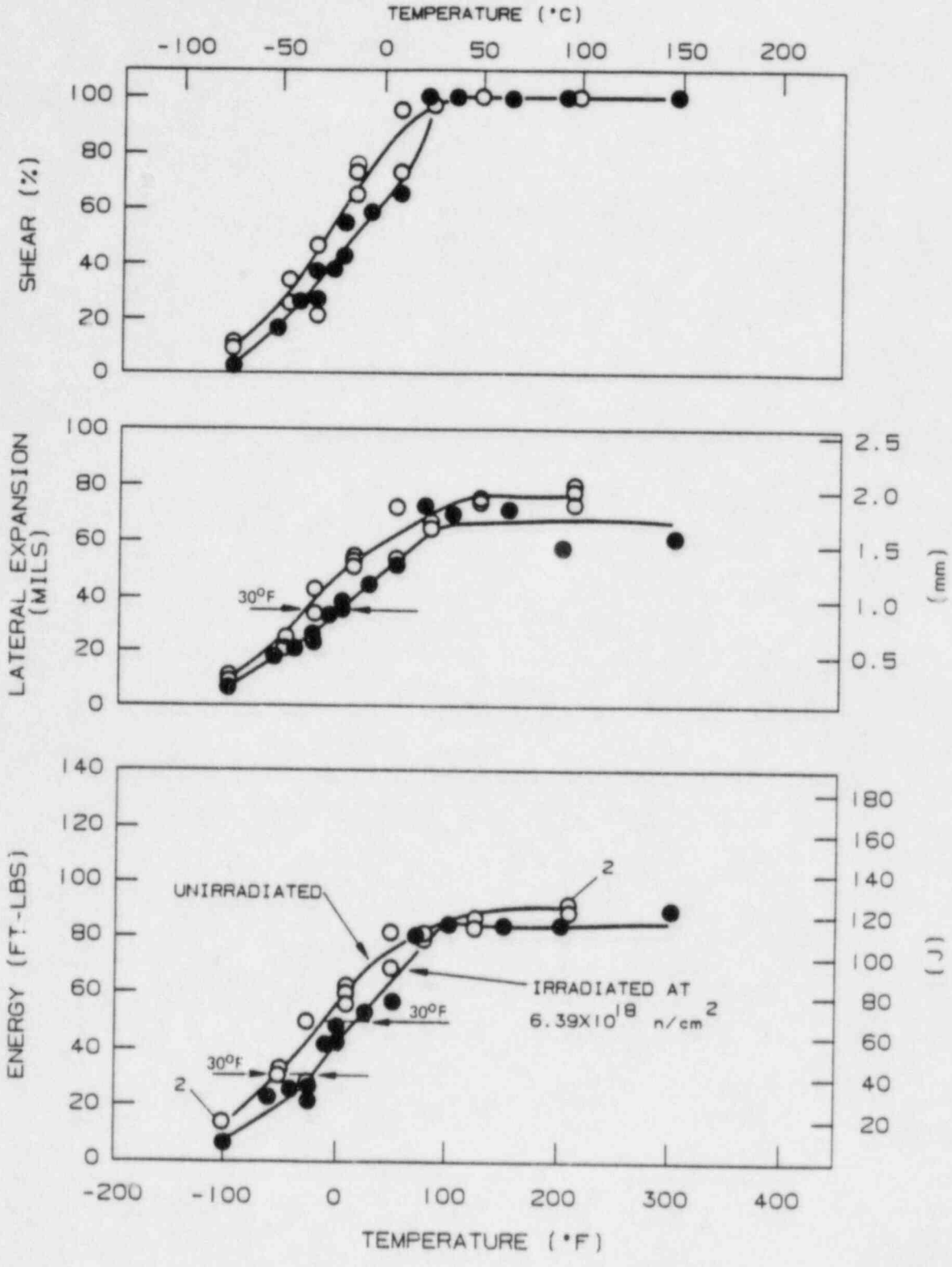

Figure 5-3 Irradiated Charpy V-Notch Impact Properties for V.C.Summer Unit 1 Reactor Pressure Vessel Weld Metal

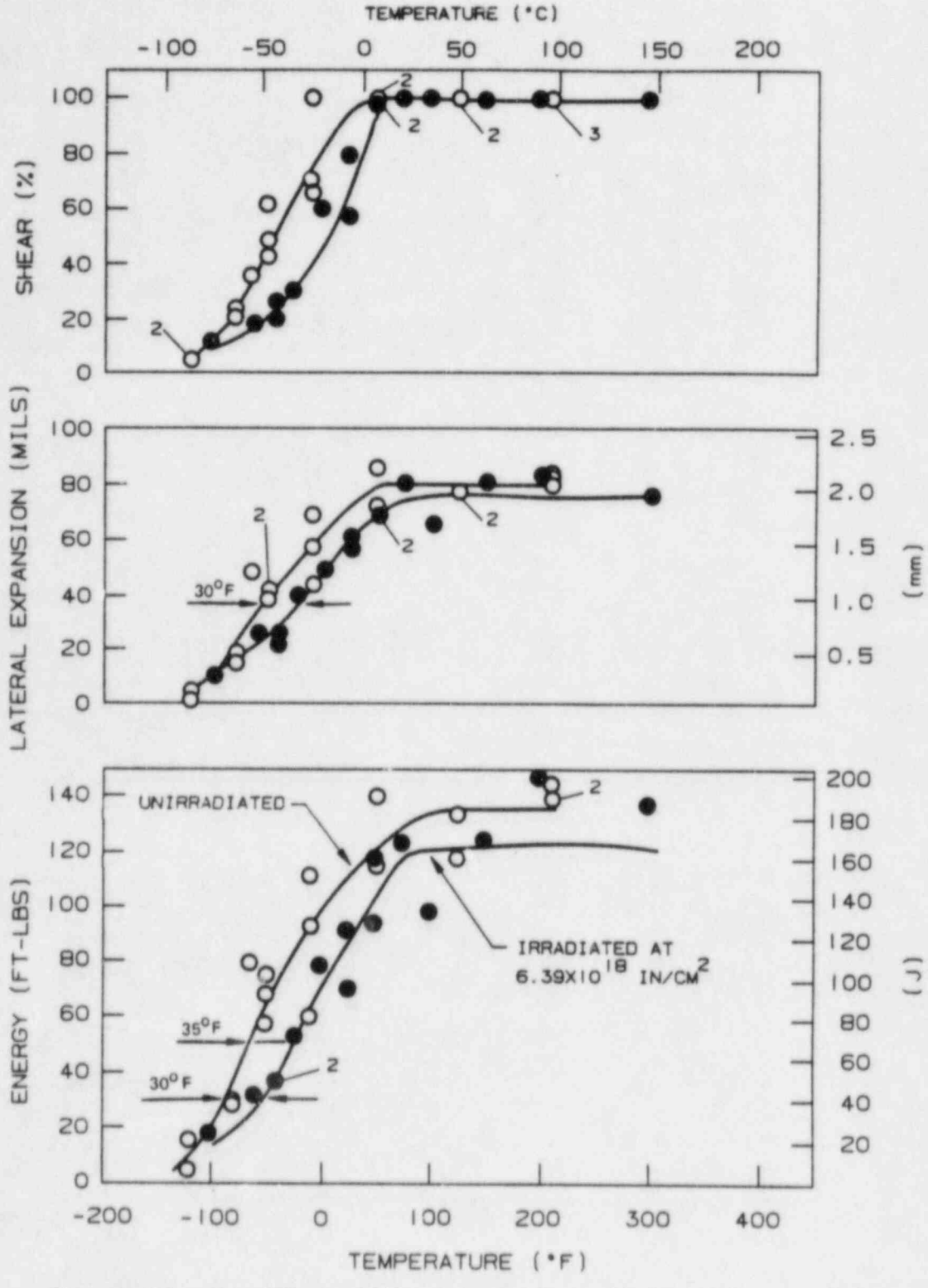

Figure 5-4 Irradiated Charpy V-Notch Impact Properties for V.C.Summer Unit 1 Reactor Pressure Vessel Weld Heat Affected Zone Metal

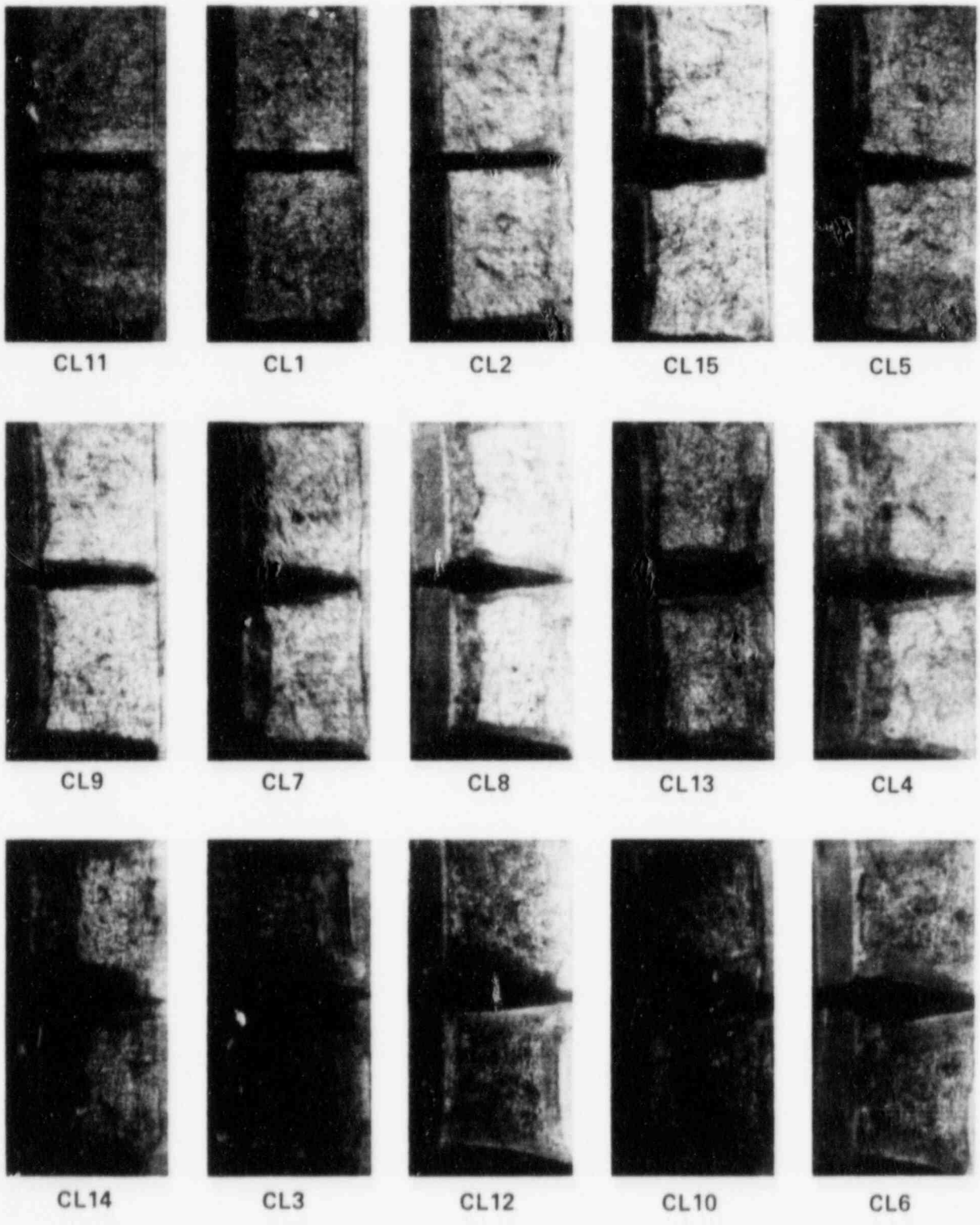

Figure 5-5. Charpy Impact Specimen Fracture Surfaces for V.C. Summer Unit 1 Reactor Pressure Vessel Intermediate Shell Plate A9154-1 (Longitudinal Orientation)

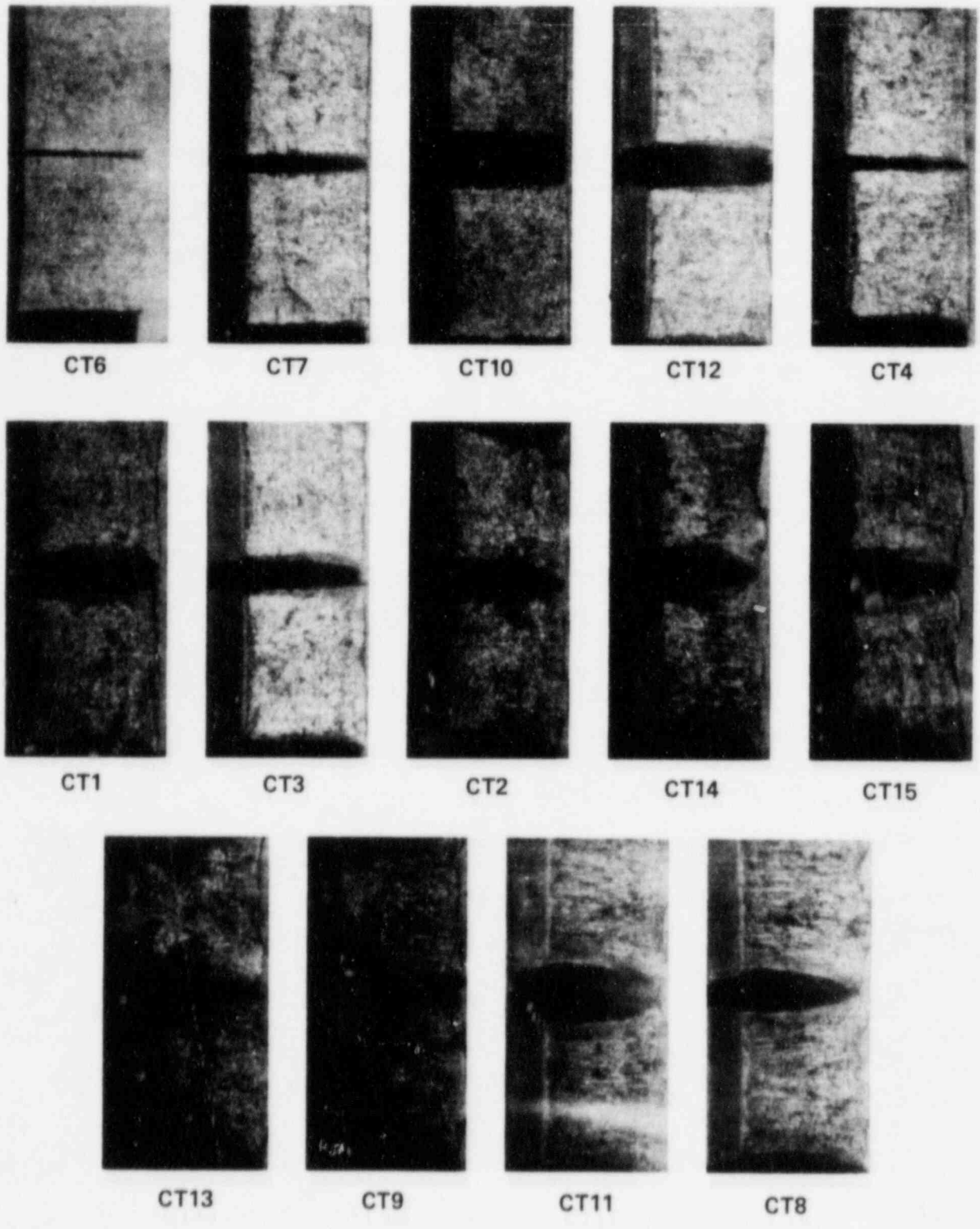

Figure 5-6. Charpy Impact Specimen Fracture Surfaces for V.C. Summer Unit 1 Reactor Pressure Vessel Intermediate Shell Plate A9154-1 (Transverse Orientation)

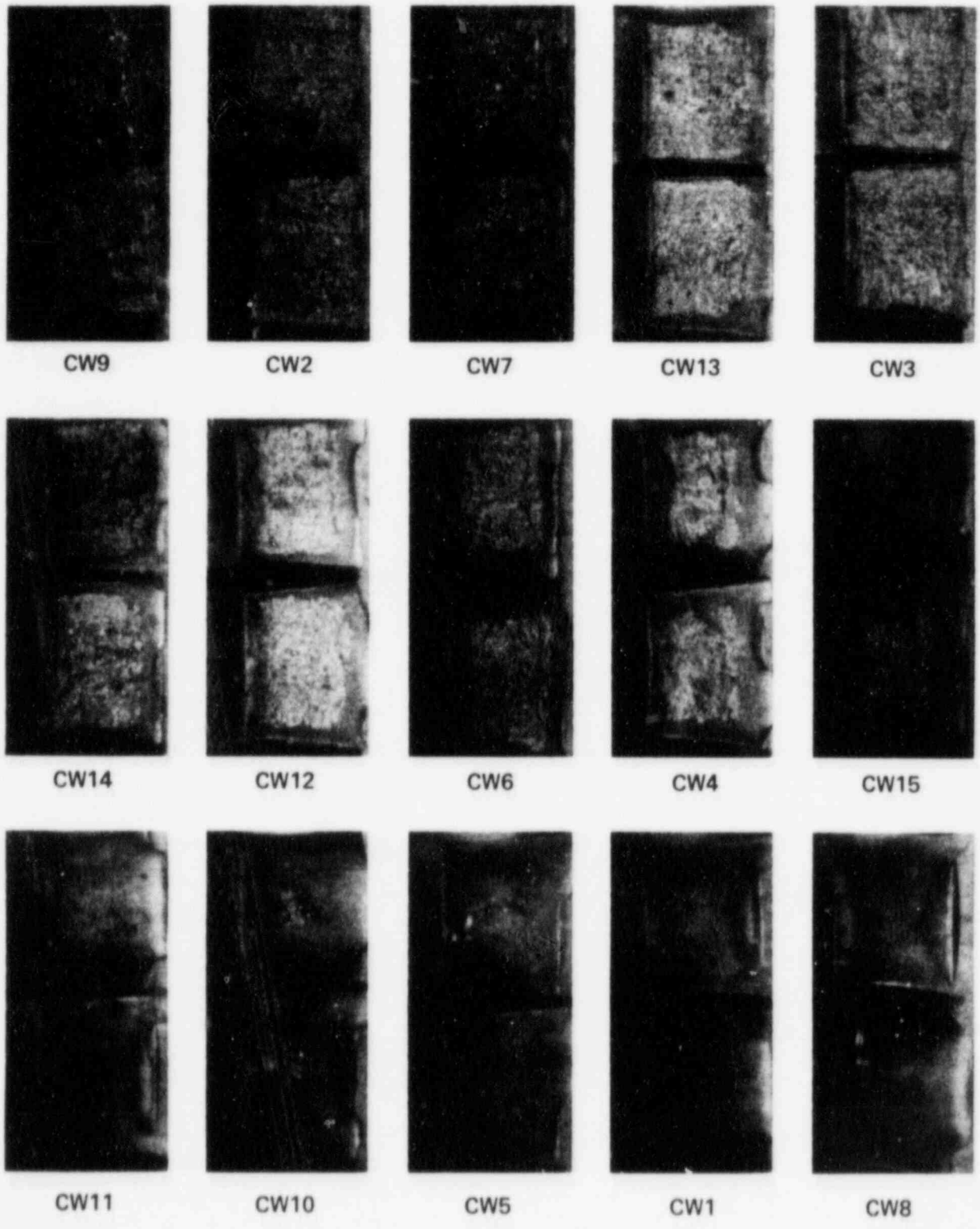

Figure 5-7. Charpy Impact Specimen Fracture Surfaces for V.C. Summer Unit 1 Weld Metal

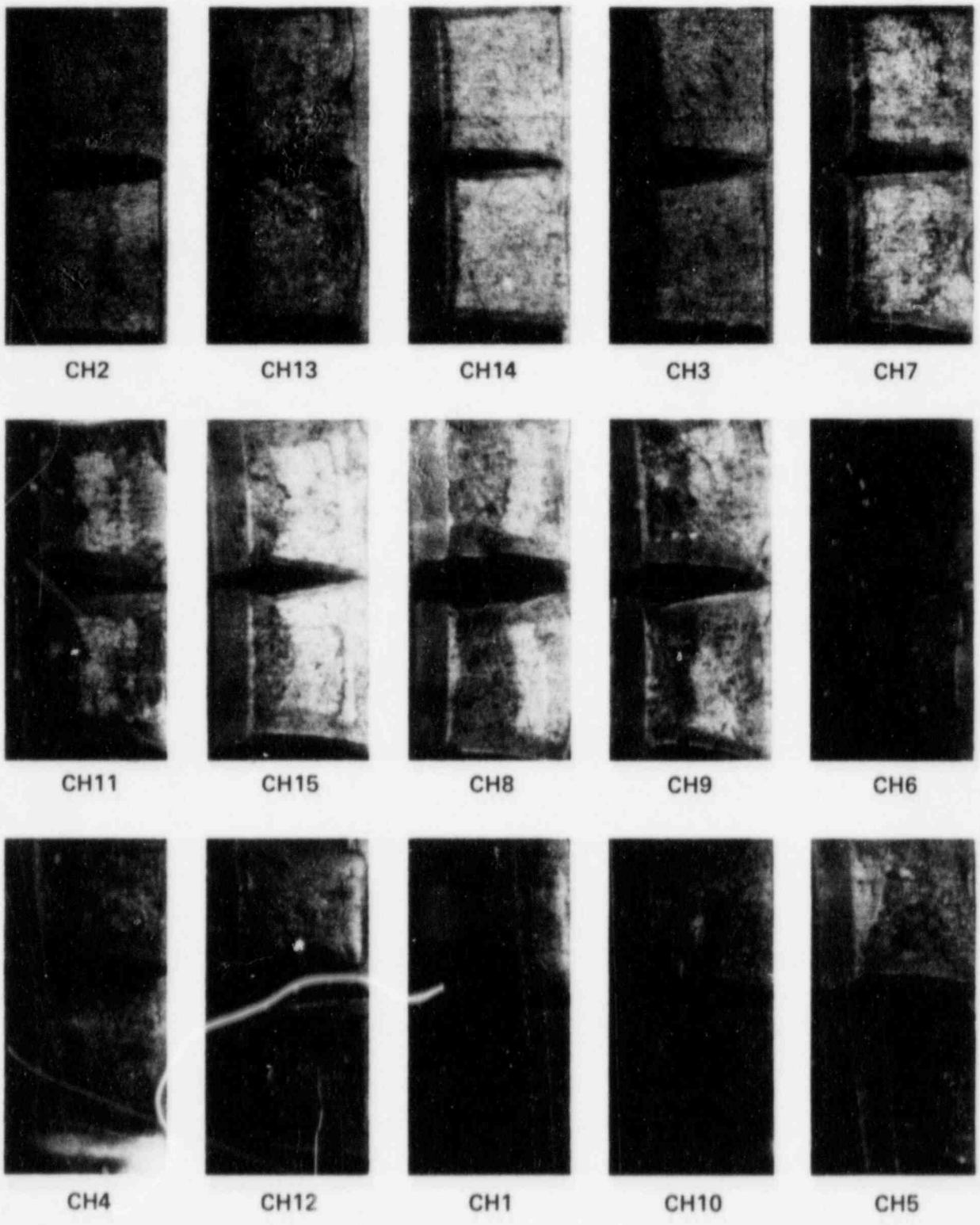

Figure 5-8. Charpy Impact Specimen Fracture Surfaces for V.C. Summer Unit 1 Weld Heat Affected Zone Metal

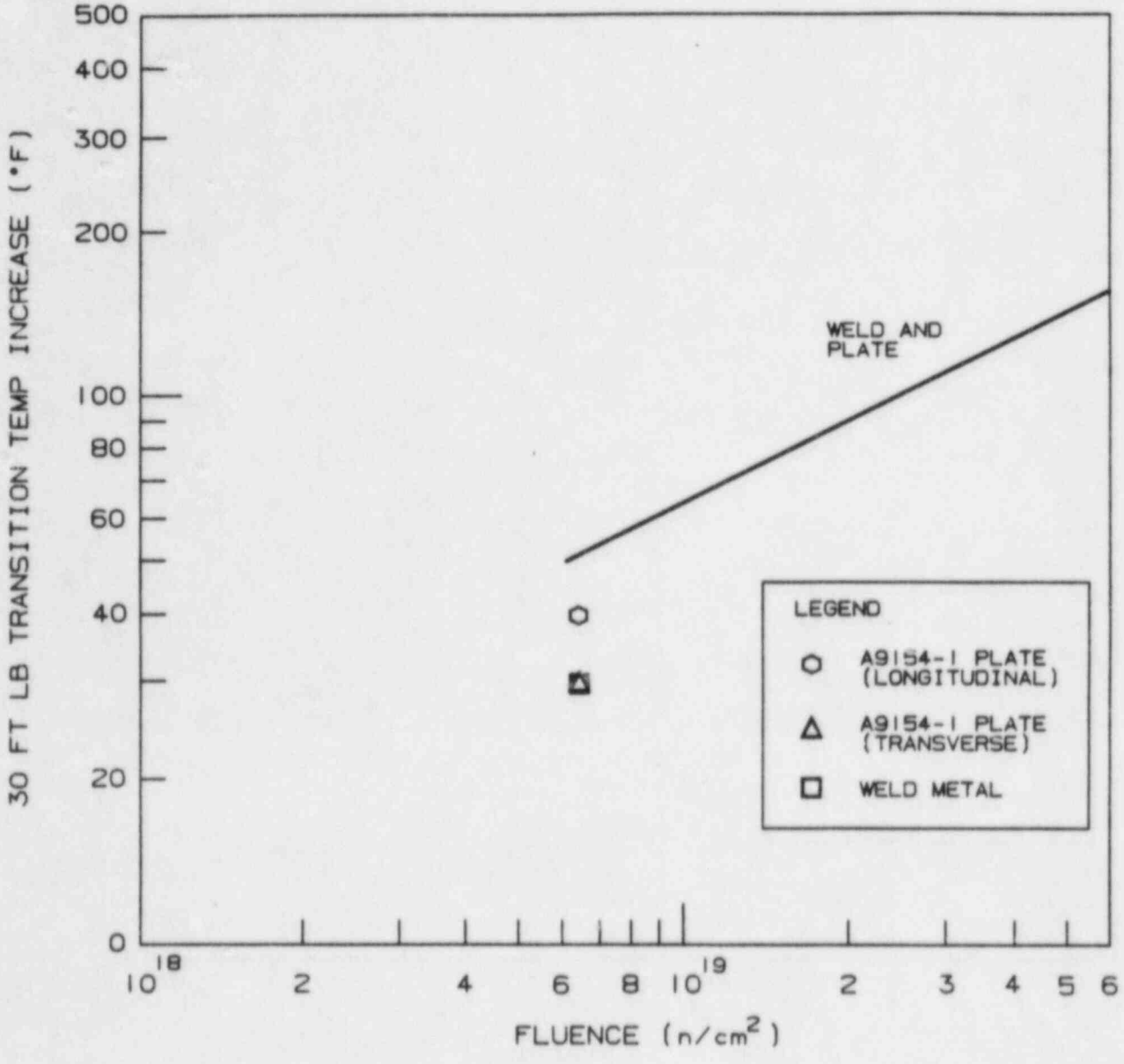

Figure 5-9 Comparison of Actual versus Predicted 30 ft-lb Transition Temperature Increases for the V.C.Summer Unit 1 Reactor Vessel Material Based on the Prediction Methods of Regulatory Guide 1.99 Revision 1

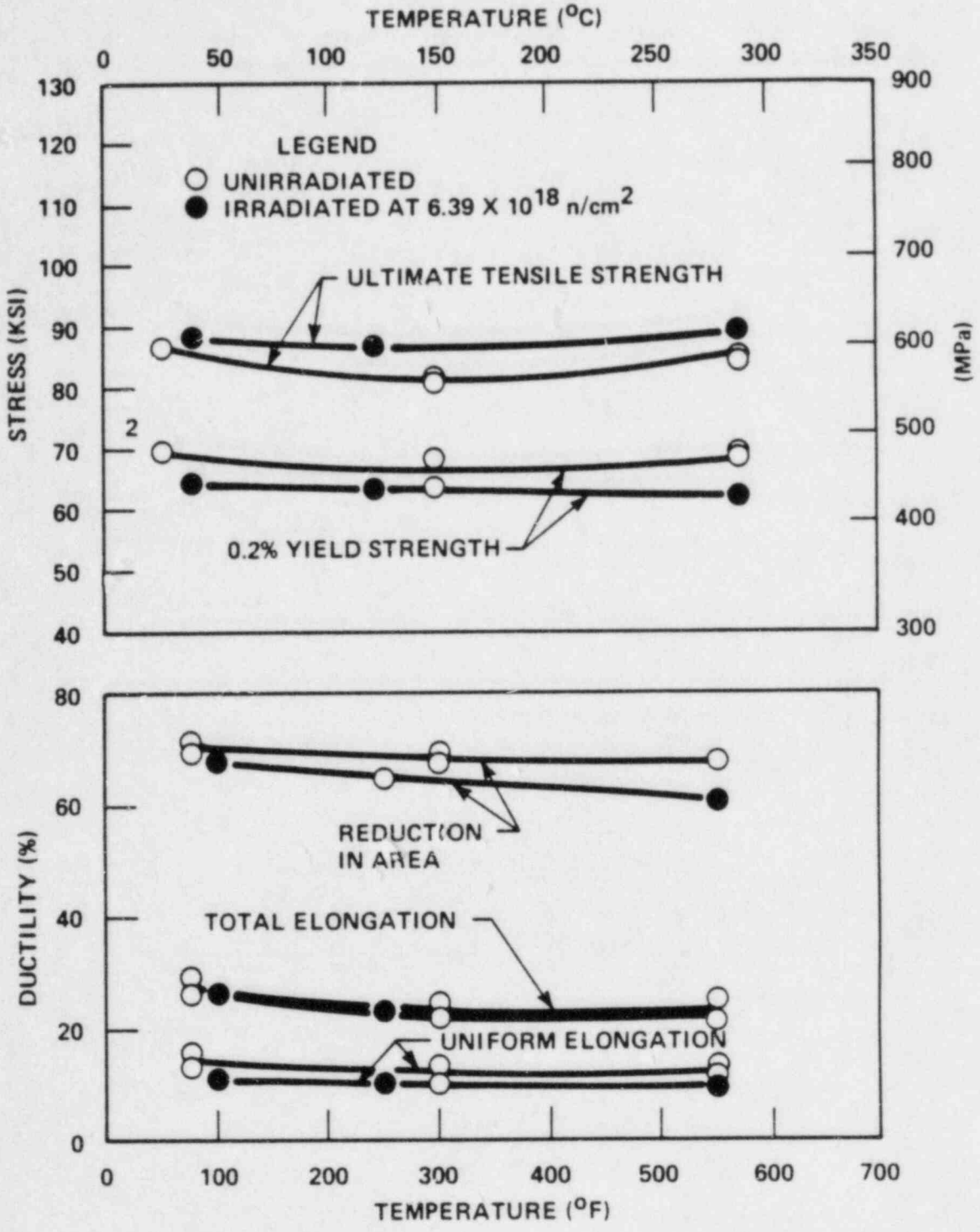

Figure 5-10. Tensile Properties for V.C. Summer Unit 1 Reactor Vessel Intermediate Shell Plate A9154-1 (Longitudinal)

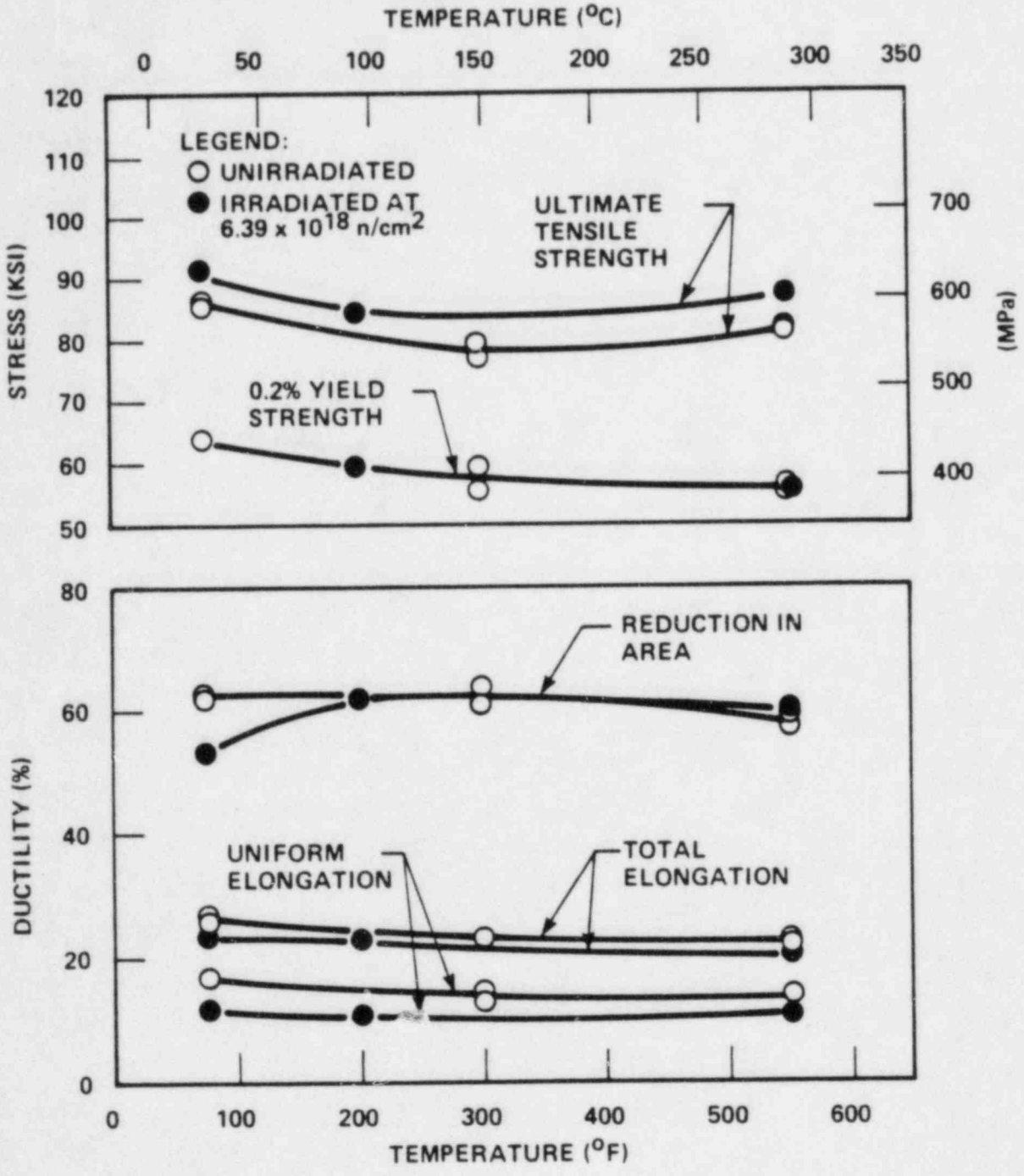

Figure 5-11. Tensile Properties for V.C. Summer Unit 1 Reactor Vessel Intermediate Shell Plate A9154-1 (Transverse)

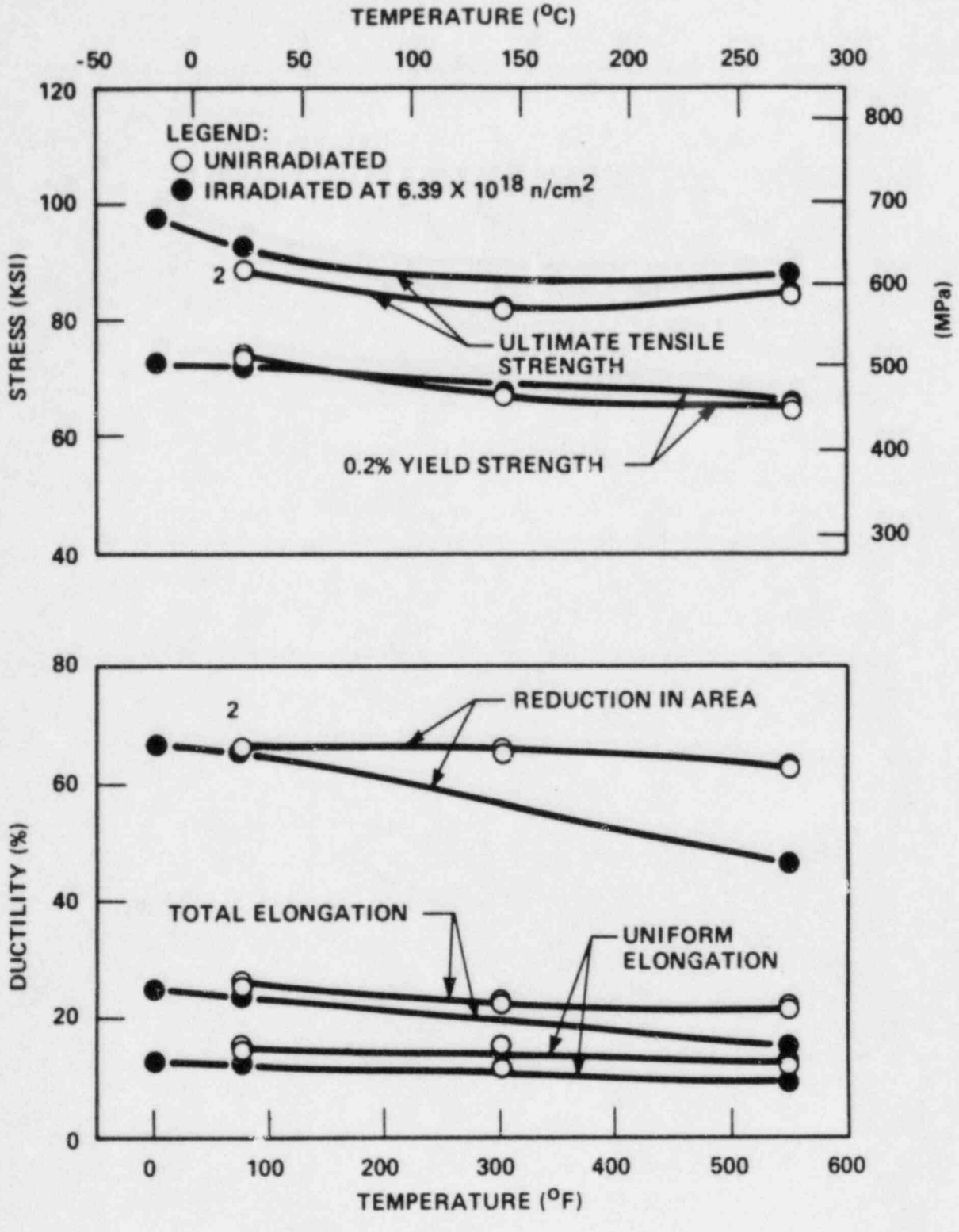

Figure 5-12. Tensile Properties for V.C. Summer Unit 1 Reactor Vessel Weld Metal

TENSILE SPECIMEN CT1
TESTED AT 74°F

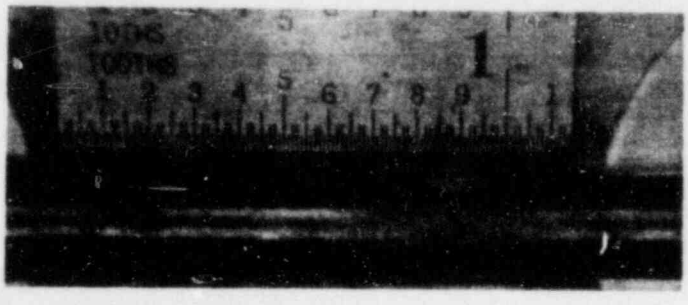

TENSILE SPECIMEN CT3
TESTED AT 200°F

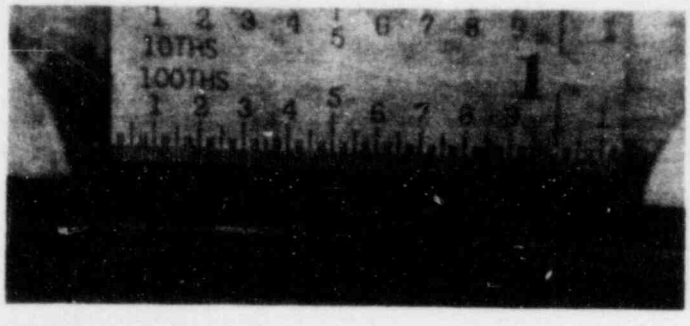

TENSILE SPECIMEN CT2
TESTED AT 550°F

Figure 5-13. Fractured Tensile Specimens of the V.C. Summer Unit 1 Reactor Vessel Intermediate Shell Plate A9154-1 (Longitudinal Orientation)

TENSILE SPECIMEN CL2
TESTED AT 100°F

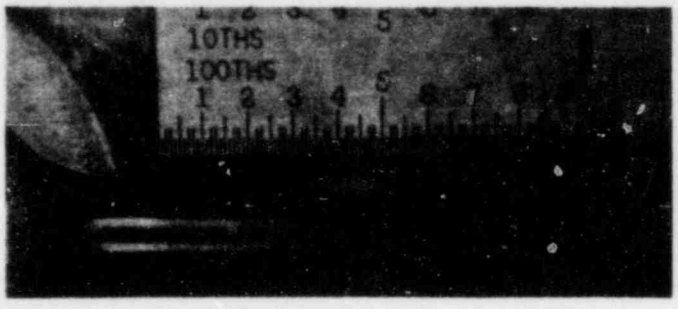

TENSILE SPECIMEN CL1
TESTED AT 250°F

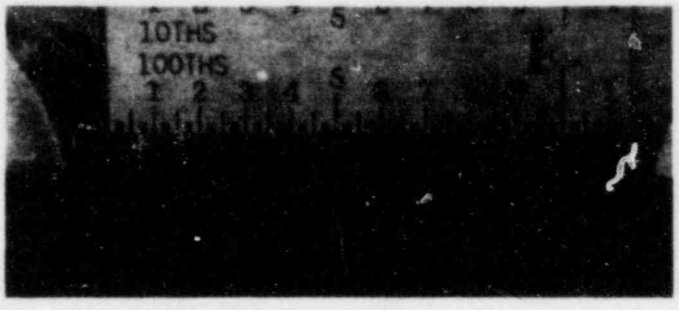

TENSILE SPECIMEN CL3
TESTED AT 550°F

Figure 5-14. Fractured Tensile Specimens of the V.C. Summer Unit 1 Reactor Vessel Intermediate Shell Plate A9154-1 (Transverse Orientation)

TENSILE SPECIMEN CW2
TESTED AT 0°F

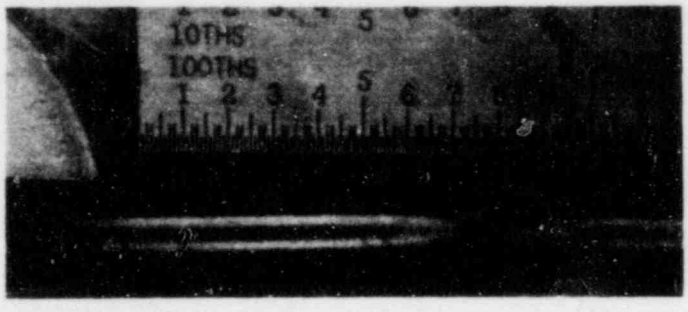

TENSILE SPECIMEN CW3
TESTED AT 74°F

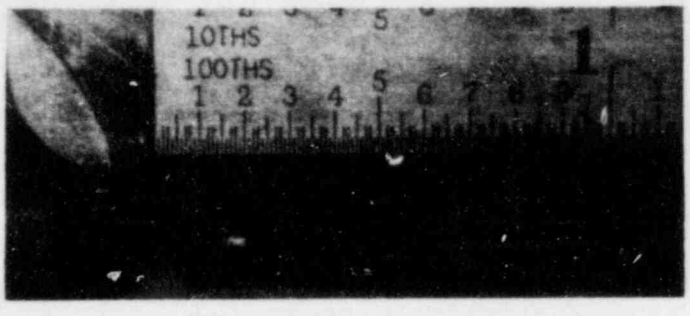

TENSILE SPECIMEN CW7
TESTED AT 550°F

NOTE: SPECIMEN BROKE
AT EXTENSOMETER
KNIFE EDGE

Figure 5-15. Fractured Tensile Specimens of the V.C. Summer Unit 1 Reactor Vessel Weld Metal

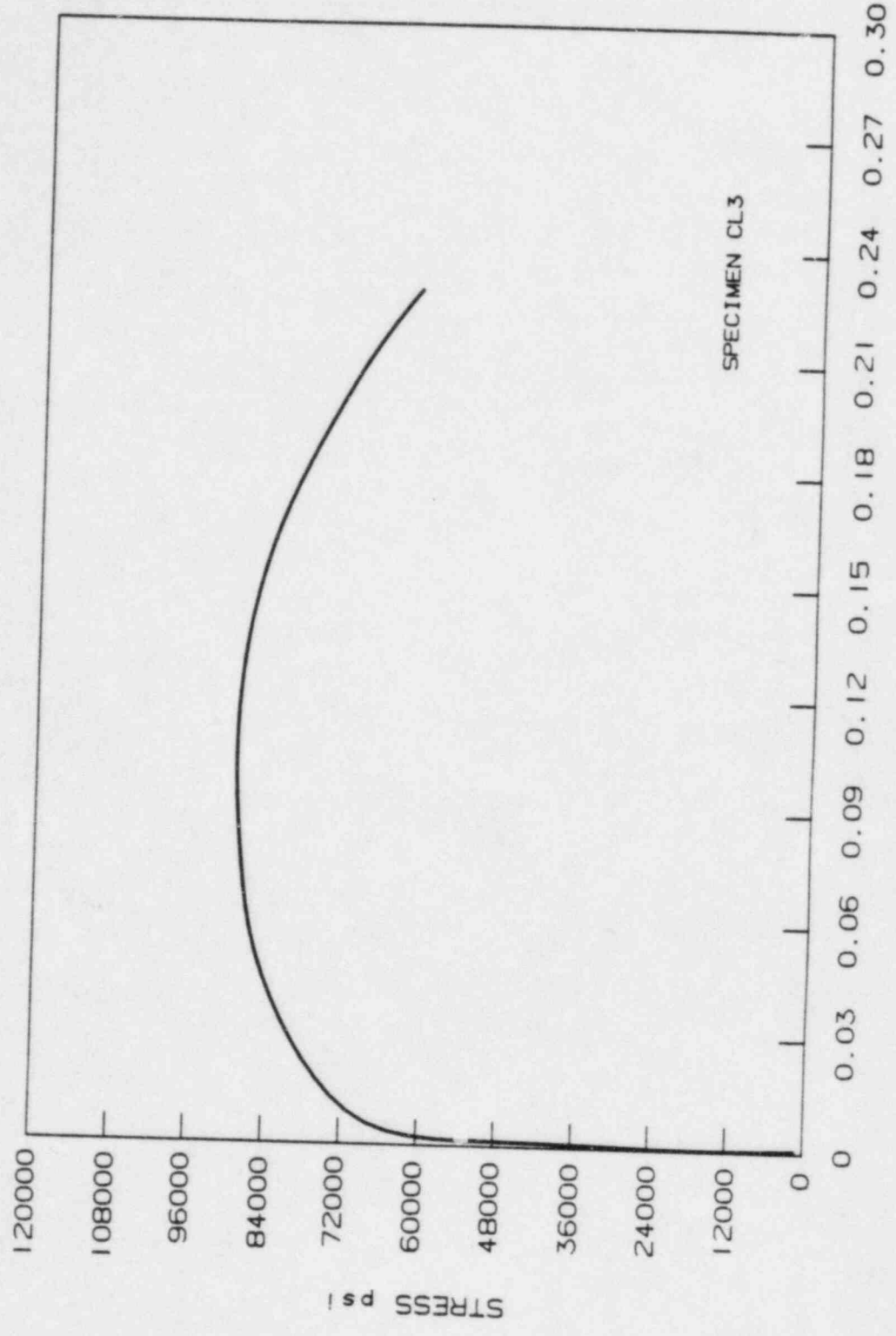

Figure 5-16 Typical Stress-Strain Curve for Tensile Specimens

SECTION 6
RADIATION ANALYSIS AND NEUTRON DOSIMETRY

6-1. INTRODUCTION

Knowledge of the neutron environment within the reactor pressure vessel/surveillance capsule geometry is required as an integral part of LWR reactor pressure vessel surveillance programs for two reasons. First, in order to interpret the neutron radiation-induced material property changes observed in the test specimens, the neutron environment (energy spectrum, flux, fluence) to which the test specimens were exposed must be known. Second, in order to relate the changes observed in the test specimens to the present and future condition of the reactor vessel, a relationship must be established between the neutron environment at various positions within the reactor vessel and that experienced by the test specimens. The former requirement is normally met by employing a combination of rigorous analytical techniques and measurements obtained with passive neutron flux monitors contained in each of the surveillance capsules. The latter information is derived solely from analysis.

This section describes a discrete ordinates S_n transport analysis performed for the V. C. Summer reactor to determine the fast ($E > 1.0$ MeV) neutron flux and fluence as well as the neutron energy spectra within the reactor vessel and surveillance capsules. The analytical data were then used to develop lead factors for use in relating neutron exposure of the reactor vessel to that of the surveillance capsules. Based on the use of spectrum-averaged reaction cross sections derived from this calculation and the V. C. Summer power history, the analysis of the neutron dosimetry contained in Capsule U is presented.

6-2. DISCRETE ORDINATES ANALYSIS

A plan view of the V. C. Summer reactor geometry at the core midplane is shown in figure 6-1. Since the reactor exhibits 1/8th core symmetry, only a zero- to 45-degree sector is depicted. Six irradiation capsules attached to

the neutron pad are included in the reactor design to constitute the reactor vessel surveillance program. The capsules are located at 16.94 degrees (U,V,X) and 19.72 degrees (W,Y,Z) from the cardinal axes as shown in figure 6-1.

A plan view of a dual surveillance capsule holder attached to the neutron pad is shown in figure 6-2. The stainless steel specimen containers are approximately 1-inch square and approximately 56 inches in height. The containers are positioned axially such that the specimens are centered on the core midplane, thus spanning the central 5 feet of the 12-foot-high reactor core.

From a neutron transport standpoint, the surveillance capsule structures are significant. They have a marked effect on both the distribution of neutron flux and the neutron energy spectrum in the water annulus between the neutron pad and the reactor vessel. In order to properly determine the neutron environment at the test specimen locations, the capsules themselves must be included in the analytical model. This requires at least a two-dimensional calculation.

In the analysis of the neutron environment within the V. C. Summer reactor geometry, predictions of neutron flux distributions and energy spectra were made with the DOT[5] two-dimensional discrete ordinates transport code. The radial and azimuthal distributions were obtained from an R,θ calculation wherein the geometry shown in figures 6-1 and 6-2 was represented in the analytical model. In addition to the R,θ calculation, a second calculation in R,Z geometry was also carried out to obtain relative axial variations of neutron flux throughout the geometry of interest. In the R,Z analysis, the reactor core was treated as an equivalent volume cylinder. The surveillance capsules were not included in the R,Z model.

Both the R,θ and R,Z analyses employed 47 neutron energy groups and a P_3 expansion of the scattering cross sections. The cross sections used in the analyses were obtained from the SAILOR cross section library[6] which was developed specifically for light water reactor applications. The neutron energy group structure used in the analysis is listed in table 6-1.

A key input parameter in the analysis of the integrated neutron exposure of the reactor vessel is the core power distribution. For this analysis, core power distributions representative of time-averaged conditions derived from statistical studies of long-term operation of Westinghouse 3-loop plants were employed. These input distributions include rod-by-rod spatial variations for all peripheral fuel assemblies.

This generic, design basis, core power distribution is intended to provide a vehicle for the long-term (end-of-life) projection of reactor vessel exposure. Since plant-specific core power distributions reflect only past operation, their use for projection into the future may not be justified. The use of generic data which reflects long-term operation of similar reactor cores may provide a more suitable approach.

Benchmark testing of these generic core power distributions and the SAILOR cross sections against surveillance capsule data obtained from two-, three-, and four-loop Westinghouse plants indicate that this analytical approach yields conservative results, with calculations exceeding measurements from 10 to 25 percent.[7]

One further point of interest regarding these analyses is that the design basis assumes an out-in fuel loading pattern (fresh fuel on the periphery). Future commitment to low-leakage core loading patterns could significantly reduce the calculated neutron flux levels presented in section 6-4. In addition, surveillance capsule lead factors could be changed, thereby influencing the withdrawal schedule of the remaining surveillance capsules.

Having the results of the R,θ and R,Z calculations, three-dimensional variations of neutron flux may be approximated by assuming that the following relation holds for the applicable regions of the reactor.

$$\phi(R,Z,\theta,E_g) = \phi(R,\theta,E_g) \times F(Z,E_g) \qquad (6\text{-}1)$$

where

$\phi(R,Z,\theta,E_g)$ = neutron flux at point R,Z,θ within energy group g

$\phi(R,\theta,E_g)$ = neutron flux at point R,θ within energy group g obtained from the R,θ calculation

$F(Z,E_g)$ = relative axial distribution of neutron flux within energy group g obtained from the R,Z calculation

This analysis is consistent with established ASTM standards.[8,9,10,11,12]

6-3. RADIOMETRIC MONITORS

The passive radiometric monitors included in the V. C. Summer surveillance program are listed in table 6-2. The first five reactions in table 6-2 are used as fast neutron monitors to relate fast (E > 1.0 MeV) neutron fluence to measured material property changes. In order to address the potential for burnout of the product nuclides generated by fast neutron reactions, it is necessary to also determine the magnitude of the thermal and resonance region neutron fluxes at the monitor location. Therefore, bare and cadmium-shielded cobalt-aluminum monitors are also included.

The relative locations of the various radiometric monitors within the surveillance capsule are shown in figure 4-2. The iron, nickel, copper, and cobalt-aluminum monitors, in wire form, are placed in holes drilled in spacers at several axial levels within the capsules. The cadmium-shielded neptunium and uranium fission monitors are accommodated within the dosimeter block located near the axial center of the capsule. All monitors are located radially at the center of the capsule and azimuthally within $\pm$ 0.23 degrees of the capsule center.

The use of passive monitors such as those listed in table 6-2 does not yield a direct measure of the energy-dependent neutron flux level at the point of interest. Rather, the activation or fission process is a measure of the integrated effect that the time- and energy-dependent neutron flux has on the

target material over the course of the irradiation period. An accurate assessment of the average neutron flux level incident on the various monitors may be derived from the activation measurements only if the irradiation parameters are well known. In particular, the following variables are important.

- o The operating history of the reactor
- o The energy response of the monitor
- o The neutron energy spectrum at the monitor location
- o The physical characteristics of the monitor

The analysis of the passive monitors and the subsequent derivation of the average neutron flux requires two operations. First, the disintegration rate of product nuclide per unit mass of monitor must be determined. Second, in order to define a suitable spectrum-averaged reaction cross section, the neutron energy spectrum at the monitor location must be calculated.

The specific activity of each of the monitors is determined using established ASTM procedures.[13,14,15,16,17,18,19,20,21] Following sample preparation, the activity of each monitor is determined by means of a lithium-drifted germanium, Ge(Li), gamma ray spectrometer. The overall standard deviation of the measured data is a function of the precision of sample weighing, the uncertainty in counting, and the acceptable error in detector calibration. For the samples removed from V. C. Summer, the overall 2σ deviation in the measured data is determined to be plus or minus 10 percent. The neutron energy spectrum at the monitor location is determined analytically using the method described in paragraph 6-2.

Having the measured activity of the monitors and the neutron energy spectrum at the monitor locations of interest, the calculation of the neutron flux proceeds as follows. The reaction product activity in the monitor is expressed as

$$A = N_o F Y \int_E \sigma(E)\, \phi(E)\, dE \sum_{j=1}^{n} \frac{P_j}{P_{max}} (1 - e^{-\lambda t_j})\, e^{-\lambda t_d} \qquad (6\text{-}2)$$

where

A	= induced product activity (dps per gram)
N_o	= number of target element atoms per gram
F	= weight fraction of the target nuclide in the target material
Y	= number of product atoms produced per reaction
$\sigma(E)$	= energy dependent reaction cross section
$\phi(E)$	= energy dependent neutron flux at the monitor location with the reactor at full (reference) power
P_j	= average core power level during irradiation period j
P_{max}	= maximum or reference core power level
λ	= decay constant of the product nuclide
t_j	= length of irradiation period j
t_d	= decay time following irradiation period j
n	= total number of irradiation periods

Because the neutron flux distributions are calculated using multigroup transport methods and, further, because the main interest is in the fast (E > 1.0 MeV) neutron flux, spectrum-averaged reaction cross sections are defined such that the integral term in equation (6-2) is replaced by the following relation.

$$\int_E \sigma(E)\ \phi(E)\ dE = \bar{\sigma}\ \Phi_f$$

where

$$\bar{\sigma} = \frac{\int_0^\infty \sigma(E)\ \phi(E)\ dE}{\int_{1\ MeV}^\infty \phi(E)\ dE} = \frac{\sum_{g=1}^{47} \sigma_g\ \Phi_g}{\sum_{g=1}^{18} \Phi_g}$$

$$\Phi_f = \int_{1\ MeV}^\infty \phi(E)\ dE = \sum_{g=1}^{18} \Phi_g$$

g = group number from Table 6-1

Thus, equation (6-2) is rewritten

$$A = N_o F Y \bar{\sigma} \Phi_f \sum_{j=1}^{n} \frac{P_j}{P_{max}} (1-e^{-\lambda t_j}) e^{-\lambda t_d}$$

or, solving for the fast (E > 1.0 MeV) neutron flux,

$$\Phi_f = \frac{A}{N_o F Y \bar{\sigma} \sum_{j=1}^{n} \frac{P_j}{P_{max}} (1-e^{-\lambda t_j}) e^{-\lambda t_d}} \qquad (6-3)$$

The total fast (E > 1.0 MeV) neutron fluence is then given by

$$\Phi_f = \Phi_f \sum_{j=1}^{n} \frac{P_j}{P_{max}} t_j \qquad (6-4)$$

where

$\sum_{j=1}^{n} \frac{P_j}{P_{max}} t_j$ = total effective full power seconds of reactor operation up to the time of capsule removal

An assessment of the potential for product nuclide burnout may be made using the bare and cadmium shielded cobalt measured activities and published data for the 2200 m/s absorption cross-section and the resonance integral This is done by rewriting equation (6-2) in terms of a monitor 2200 m/s neutron flux and a monitor resonance flux as follows:

$$A_{bare} = N_o F Y (\sigma_{2200} \Phi_{2200} + RI \Phi_{res}) \sum_{j=1}^{n} \frac{P_j}{P_{max}} (1-e^{-\lambda t_j}) e^{-\lambda t_d} \qquad (6-5)$$

$$A_{cd} = N_o F Y (RI \Phi_{res}) \sum_{j=1}^{n} \frac{P_j}{P_{max}} (1 - e^{-\lambda t_j}) e^{-\lambda t_d} \qquad (6-6)$$

A_{bare} = bare induced product activity (dps per gram)

A_{cd} = cadmium shielded induced product activity (dps per gram)

σ_{2200} = published 2200 m/s absorption cross-section for nuclide of interest

RI = published epicadmium dilute resonance integral for nuclide of interest

Φ_{2200} = monitor 2200 m/s neutron flux to be determined from measured activities

Φ_{res} = monitor resonance neutron flux to be determined from measured activities

Equations (6-5) and (6-6) are solved for Φ_{2200} and Φ_{res} using the average measured bare and cadmium shielded cobalt activities at the monitor location.

The total loss rate of a product nuclide may then be expressed as the sum of its radioactive decay rate and the neutron absorption rate in that nuclide while the reactor is at power. The product nuclide neutron absorption rate may be estimated from the published data for σ_{2200} and RI and the monitor fluxes determined above. If the neutron absorption rate is small when compared to the decay rate then there is no concern regarding burnout.

6-4. NEUTRON TRANSPORT ANALYSIS RESULTS

Results of the discrete ordinates transport calculations for the V. C. Summer reactor are summarized in this section. In figure 6-3, the calculated maximum fast (E > 1.0 MeV) neutron flux levels at the radius of the surveillance capsule center, the reactor vessel inner radius, the reactor vessel 1/4 thickness location, and the reactor vessel 3/4 thickness location are

presented as a function of azimuthal angle. The local influence of the surveillance capsules on the fast neutron flux distribution is clearly evident. In figure 6-4, the radial distribution of maximum fast (E > 1.0 MeV) neutron flux through the thickness of the reactor vessel is shown. The relative axial variation of fast neutron flux within the reactor vessel is given in figure 6-5. Absolute axial variations of fast neutron flux may be obtained by multiplying the levels given in figure 6-3 or 6-4 by the appropriate values from figure 6-5. Table 6-3 provides the calculated fast neutron exposure parameters for the V. C. Summer reactor vessel.

Table 6-4 provides the calculated fast neutron exposure parameters and updated lead factors for all of the V. C. Summer surveillance capsules. The lead factor is defined as the ratio of the fast (E > 1.0 MeV) neutron flux at the dosimeter block location (capsule center) to the maximum fast neutron flux at the reactor vessel inner radius. Table 6-5 provides the calculated fast neutron exposure parameters for the various metallurgical specimens within V. C. Summer surveillance capsule U.

In order to derive neutron flux and fluence levels from the measured disintegration rates, suitable spectrum-averaged reaction cross sections are required. The calculated neutron energy spectrum at the center of the V. C. Summer surveillance capsule U is listed in table 6-6. The calculated spectrum-averaged cross sections for each of the fast neutron reactions are given in table 6-7.

6-5. DOSIMETRY RESULTS

The irradiation history of the V. C. Summer reactor up to the time of removal of Capsule U is listed in table 6-8. Comparisons of measured and calculated saturated activity of the radiometric monitors contained in Capsule U based on the irradiation history shown in table 6-8 are listed in table 6-9.

The fast (E > 1.0 MeV) neutron flux and fluence levels derived for Capsule U using the spectrum averaged cross-sections listed in table 6-7 are presented

in table 6-10. Table 6-11 summarizes the key nuclear data and results of the product nuclide burnout assessment that was performed. Due to the relatively low thermal and resonance neutron fluxes at the surveillance capsule location, the neutron absorption rate is negligably small when compared to the radioactive decay rate. Therefore, no correction has been made for product nuclide burnout.

An examination of table 6-10 shows that the average fast (E > 1.0 MeV) neutron flux derived from the five threshold reactions is 1.80×10^{11} n/cm^2-sec with a 1σ standard deviation of $\pm$7.5 percent. The calculated flux value of 2.09×10^{11} n/cm^2-sec exceeds all of the measured values, with calculation to experimental ratios ranging from 1.06 to 1.25.

A summary of measured and calculated current fast neutron exposures for Capsule U and for key reactor vessel locations is presented in table 6-12. The measured value is given based on the average of all five threshold reactions listed in table 6-10. End-of-life (EOL) reactor vessel fast neutron fluence projections are also included in table 6-12.

Based on the data given in table 6-10, the best estimate fast neutron exposure of Capsule U is

$$\Phi = 6.39 \times 10^{18} \text{ n/cm}^2 \text{ (E > 1 MeV) at 1.12 EFPY.}$$

TABLE 6-1

SAILOR 47 NEUTRON ENERGY GROUP STRUCTURE

Energy Group	Group Lower Energy (MeV)	Energy Group	Group Lower Energy (MeV)
1	14.19[a]	25	0.183
2	12.21	26	0.111
3	10.00	27	0.0674
4	8.61	28	0.0409
5	7.41	29	0.0318
6	6.07	30	0.0261
7	4.97	31	0.0242
8	3.68	32	0.0219
9	3.01	33	0.0150
10	2.73	34	7.10×10^{-3}
11	2.47	35	3.36×10^{-3}
12	2.37	36	1.59×10^{-3}
13	2.35	37	4.54×10^{-4}
14	2.23	38	2.14×10^{-4}
15	1.92	39	1.01×10^{-4}
16	1.65	40	3.73×10^{-5}
17	1.35	41	1.07×10^{-5}
18	1.00	42	5.04×10^{-6}
19	0.821	43	1.86×10^{-6}
20	0.743	44	8.76×10^{-7}
21	0.608	45	4.14×10^{-7}
22	0.498	46	1.00×10^{-7}
23	0.369	47	0.00
24	0.298		

a) The upper energy of group 1 is 17.33 MeV.

TABLE 6-2

NUCLEAR CONSTANTS FOR RADIOMETRIC MONITORS CONTAINED IN THE V. C. SUMMER SURVEILLANCE CAPSULES

Monitor Material	Reaction of Interest	Target Weight Fraction	Product Half-life	Fission Yield (%)
Iron wire	Fe^{54} (n,p) Mn^{54}	0.058	312.2 dy	
Nickel wire	Ni^{58} (n,p) Co^{58}	0.6827	70.91 dy	
Copper wire	Cu^{63} (n,α) Co^{60}	0.6917	5.272 yr	
Uranium-238[a] in U_3O_8	U^{238} (n,f) Cs^{137}	1.0	30.17 yr	6.0
Neptunium-237[a] in NpO_2	Np^{237} (n,f) Cs^{137}	1.0	30.17 yr	6.5
Cobalt-aluminum[a] wire	Co^{59} (n,γ) Co^{60}	0.0015	5.272 yr	
Cobalt-aluminum wire	Co^{59} (n,γ) Co^{60}	0.0015	5.272 yr	

a) Denotes that the monitor is cadmium-shielded

TABLE 6-3

CALCULATED FAST NEUTRON EXPOSURE PARAMETERS FOR THE PEAK LOCATION OF THE V. C. SUMMER REACTOR VESSEL

Radial Location[a] Within the Reactor Vessel	Fast Neutron Flux (n/cm^2-sec) (E > 1.0 MeV)	Fast Neutron Flux (n/cm^2-sec) (E > 0.1 MeV)	Iron Displacement Rate (dpa/sec)
Inner Surface (R = 78.500 inches)	6.73×10^{10}	1.63×10^{11}	1.07×10^{-10}
1/4 Thickness (R = 80.469 inches)	3.99×10^{10}	1.44×10^{11}	7.27×10^{-11}
1/2 Thickness (R = 82.438 inches)	1.98×10^{10}	1.05×10^{11}	4.49×10^{-11}
3/4 Thickness (R = 84.406 inches)	9.26×10^{9}	6.83×10^{10}	2.64×10^{-11}
Outer Surface (R = 86.375 inches)	3.81×10^{9}	3.46×10^{10}	1.28×10^{-11}

a) The peak is located at zero degrees azimuthally and on the core midplane.

TABLE 6-4

CALCULATED FAST NEUTRON EXPOSURE PARAMETERS AND
LEAD FACTORS FOR THE V. C. SUMMER SURVEILLANCE CAPSULES

Capsule I.D.	Azimuthal Location[a] (Degrees)	Fast Neutron Flux (n/cm^2-sec) (E > 1.0 MeV)	Fast Neutron Flux (n/cm^2-sec) (E > 0.1 MeV)	Iron Displacement Rate (dpa/sec)	Lead Factor[b]
V	106.94	2.09×10^{11}	1.05×10^{12}	4.47×10^{-10}	3.11
W	109.72	1.81×10^{11}	8.80×10^{11}	3.80×10^{-10}	2.69
X	286.94	2.09×10^{11}	1.05×10^{12}	4.47×10^{-10}	3.11
Y	289.72	1.81×10^{11}	8.80×10^{11}	3.80×10^{-10}	2.69
Z	340.28	1.81×10^{11}	8.80×10^{11}	3.80×10^{-10}	2.69
U	343.06	2.09×10^{11}	1.05×10^{12}	4.47×10^{-10}	3.11

a) The radius of the surveillance center is 73.310 inches.

b) The lead factor is the ratio of the fast (E > 1.0 MeV) neutron flux at the center of the surveillance capsule to that at the peak location on the reactor vessel inner surface.

TABLE 6-5

CALCULATED FAST NEUTRON EXPOSURE PARAMETERS FOR
W. C. SUMMER SURVEILLANCE CAPSULE U METALLURGICAL SPECIMENS

Specimen Type and Location	Fast Neutron Flux (n/cm^2-sec) (E > 1.0 MeV)	Fast Neutron Flux (n/cm^2-sec) (E > 0.1 MeV)	Iron Displacement (dpa/sec)
CHARPY SPECIMENS			
R = 73.007 in. θ = 342.75 deg.	2.36×10^{11}	1.16×10^{12}	4.98×10^{-10}
θ = 343.06 deg.	2.40×10^{11}	1.18×10^{12}	5.06×10^{-10}
θ = 343.37 deg.	2.43×10^{11}	1.18×10^{12}	5.10×10^{-10}
R = 73.613 in. θ = 342.75 deg.	1.79×10^{11}	9.17×10^{11}	3.89×10^{-10}
θ = 343.06 deg.	1.82×10^{11}	9.27×10^{11}	3.93×10^{-10}
θ = 343.37 deg.	1.84×10^{11}	9.25×10^{11}	3.95×10^{-10}
TENSILE SPECIMENS			
R = 73.507 in. θ = 342.75 deg.	1.88×10^{11}	9.57×10^{11}	4.06×10^{-10}
θ = 343.06 deg.	1.91×10^{11}	9.68×10^{11}	4.11×10^{-10}
θ = 343.37 deg.	1.93×10^{11}	9.66×10^{11}	4.13×10^{-10}
PRE-CRACKED BEND BAR			
R = 73.310 in. θ = 343.06 deg.	2.09×10^{11}	1.05×10^{12}	4.47×10^{-10}
COMPACT TENSION SPECIMEN			
R = 73.060 in. θ = 343.06 deg.	2.35×10^{11}	1.15×10^{12}	4.96×10^{-10}
R = 73.560 in.	1.87×10^{11}	9.47×10^{11}	4.02×10^{-10}

TABLE 6-6

CALCULATED NEUTRON ENERGY SPECTRUM AT THE CENTER OF

V. C. SUMMER SURVEILLANCE CAPSULE U

Energy Group	Neutron Flux (n/cm^2-sec)	Energy Group	Neutron Flux (n/cm^2-sec)
1	3.00×10^{7}	25	1.29×10^{11}
2	1.11×10^{8}	26	1.42×10^{11}
3	3.89×10^{8}	27	1.18×10^{11}
4	7.17×10^{8}	28	7.38×10^{10}
5	1.21×10^{9}	29	1.96×10^{10}
6	2.71×10^{9}	30	1.04×10^{10}
7	3.80×10^{9}	31	3.16×10^{10}
8	7.95×10^{9}	32	2.25×10^{10}
9	7.46×10^{9}	33	2.96×10^{10}
10	6.27×10^{9}	34	3.63×10^{10}
11	7.61×10^{9}	35	6.65×10^{10}
12	3.81×10^{9}	36	6.74×10^{10}
13	1.16×10^{9}	37	9.04×10^{10}
14	5.90×10^{9}	38	4.54×10^{10}
15	1.64×10^{10}	39	5.04×10^{10}
16	2.25×10^{10}	40	6.95×10^{10}
17	3.60×10^{10}	41	8.04×10^{10}
18	8.62×10^{10}	42	4.26×10^{10}
19	6.58×10^{10}	43	4.37×10^{10}
20	3.06×10^{10}	44	2.41×10^{10}
21	1.21×10^{11}	45	1.61×10^{10}
22	9.51×10^{10}	46	1.68×10^{10}
23	1.28×10^{11}	47	1.68×10^{10}
24	1.29×10^{11}		

TABLE 6-7

SPECTRUM-AVERAGED REACTION CROSS SECTIONS AT THE CENTER OF V. C. SUMMER SURVEILLANCE CAPSULE U

Reaction of Interest	Spectrum-Averaged Cross Section[a] (barns)
Fe^{54} (n,p) Mn^{54}	0.0515
Ni^{58} (n,p) Co^{58}	0.0726
Cu^{63} (n,α) Co^{60}	0.000428
U^{238} (n,f) Cs^{137}	0.301
Np^{237} (n,f) Cs^{137}	3.43

a) $$\bar{\sigma} = \frac{\int_0^\infty \sigma(E)\,\phi(E)\,dE}{\int_{1\ MeV}^\infty \sigma(E)\,dE}$$

TABLE 6-8

IRRADIATION HISTORY OF V. C. SUMMER

SURVEILLANCE CAPSULE U

Month	Year	P_j (MWt)	P_{max} (MWt)	P_j/P_{max}	Irradiation Time (Days)	Decay Time (Days)
11	1982	426	2775	0.154	14	751
12	1982	872	2775	0.314	31	720
1	1983	1306	2775	0.471	31	689
2	1983	1252	2775	0.451	28	661
3	1983	759	2775	0.274	31	630
4	1983	0	2775	0.000	30	600
5	1983	355	2775	0.128	31	569
6	1983	2316	2775	0.835	30	539
7	1983	2496	2775	0.899	31	508
8	1983	2355	2775	0.848	31	477
9	1983	2421	2775	0.872	30	447
10	1983	2424	2775	0.874	31	416
11	1983	2101	2775	0.757	30	386
12	1983	1072	2775	0.386	31	355
1	1984	2674	2775	0.964	31	324
2	1984	2386	2775	0.860	29	295
3	1984	1955	2775	0.704	31	264
4	1984	165	2775	0.059	30	234
5	1984	2282	2775	0.822	31	203
6	1984	2557	2775	0.921	30	173
7	1984	1116	2775	0.402	31	142
8	1984	2471	2775	0.890	31	111
9	1984	2083	2775	0.751	28	83

CAPSULE U REMOVED

Note: 1) Decay time is referenced to 12/20/84

2) Total irradiation time is 3.55×10^7 effective full power seconds (EFPS) or 1.12 effective full power years (EFPY)

3) P_j is the average core power level during the irradiation period

TABLE 6-9

COMPARISON OF MEASURED AND CALCULATED RADIOMETRIC MONITOR SATURATED ACTIVITIES FOR V. C. SUMMER SURVEILLANCE CAPSULE U

Monitor and Axial Location[a]	Radiometric Monitor Saturated Activity (Disintegrations/Second-Gram) Measured	Basis	Calculated	C/E
Fe^{54} (n,P) Mn^{54}		(gm of wire)		
Top	5.53×10^{6}			
Middle	5.48×10^{6}			
Bottom	5.95×10^{6}			
Average[b]	5.65×10^{6} [±4.6%]		6.98×10^{6}	1.24
Ni^{58} (n,P) Co^{58}		(gm of wire)		
Top	9.21×10^{7}			
Middle	8.70×10^{7}			
Bottom	9.40×10^{7}			
Average[b]	9.10×10^{7} [±4.0%]		1.08×10^{8}	1.19
Cu^{63} (n,α) Co^{60}		(gm of wire)		
Top	5.59×10^{5}			
Middle	5.51×10^{5}			
Bottom	5.75×10^{5}			
Average[b]	5.62×10^{5} [±2.2%]		5.93×10^{5}	1.06

TABLE 6-9 (continued)

COMPARISON OF MEASURED AND CALCULATED RADIOMETRIC MONITOR SATURATED ACTIVITIES FOR V. C. SUMMER SURVEILLANCE CAPSULE U

Monitor and Axial Location[a]	Radiometric Monitor Saturated Activity (Disintegrations/Second-Gram) Measured	Basis	Calculated	C/E
U^{238} (n,f) Cs^{137} (c)		(gm of U^{238})		
Middle	1.01×10^{7}			
Corrected (d)	8.14×10^{6}		9.57×10^{6}	1.18
Np^{237} (n,f) Cs^{137} (c)		(gm of Np^{237})		
Middle	9.52×10^{7}		1.19×10^{8}	1.25
Co^{59} (n,γ) Co^{60} (c)		(gm of wire)		
Top	6.83×10^{7}			
Middle	6.95×10^{7}			
Bottom	7.05×10^{7}			
Average[b]	6.94×10^{7} [±1.6%]		7.30×10^{7}	1.05
Co^{59} (n,γ) Co^{60}		(gm of wire)		
Top	1.24×10^{8}			
Top	1.04×10^{8}			
Middle	1.27×10^{8}			
Middle	1.05×10^{8}			
Bottom	1.27×10^{8}			
Bottom	1.12×10^{8}			
Average[b]	1.16×10^{8} [±9.3%]		8.56×10^{7}	0.74

TABLE 6-9 (continued)

COMPARISON OF MEASURED AND CALCULATED RADIOMETRIC
MONITOR SATURATED ACTIVITIES FOR
V. C. SUMMER SURVEILLANCE CAPSULE U

---

a) Refer to Figure 4-2 for the locations of the various radiometric monitors.

b) The standard deviation (1σ) of the mean saturated activity is expressed as a percentage of the mean.

c) This radiometric monitor was cadmium shielded.

d) The measured value has been multiplied by 0.806 to correct for the effect of 323 ppm U^{235} and the build-in of Pu^{239}.

TABLE 6-10

RESULTS OF FAST NEUTRON DOSIMETRY FOR V. C. SUMMER
SURVEILLANCE CAPSULE U

Reaction of Interest	Radiometric Monitor Satured Activity[a] (dps/gm)		Fast (E > 1.0 MeV) Neutron Flux (n/cm^2-sec)		Current[b] Fast (E > 1.0 MeV) Neutron Fluence (n/cm^2)	
	Measured	Calculated	Measured	Calculated	Measured	Calculated
Fe^{54} (n,p) Mn^{54}	5.65×10^{6}	6.98×10^{6}	1.70×10^{11}		6.03×10^{18}	
Ni^{58} (n,p) Co^{58}	9.10×10^{7}	1.08×10^{8}	1.77×10^{11}		6.29×10^{18}	
Cu^{63} (n,α) Co^{60}	5.62×10^{5}	5.93×10^{5}	1.99×10^{11}		7.06×10^{18}	
U^{238} (n,f) Cs^{137}	8.14×10^{6}	9.57×10^{6}	1.79×10^{11}		6.36×10^{18}	
Np^{237} (n,f) Cs^{137}	9.52×10^{7}	1.19×10^{8}	1.68×10^{11}		5.97×10^{18}	
Average			1.80×10^{11} [±7.5%]	2.09×10^{11}	6.39×10^{18}	7.43×10^{18}

a) Refer to Table 6-9.

b) Total irradiation time for surveillance capsule U is 3.55×10^{7} effective full power seconds (EFPS).

TABLE 6-11

PRODUCT NUCLIDE BURNOUT ASSESSMENT
FOR V. C. SUMMER SURVEILLANCE CAPSULE U

NUCLEAR DATA[22]

Nuclide	Half-Life	σ_{2200} (barns)	RI (barns)
Mn^{54}	312.2 dy	10.0	-
Co^{58}	70.91 dy	1880	6890
Co^{59}	Stable	37.2	75.5
Co^{60}	5.272 yr	2.0	4.3
Cs^{137}	30.17 yr	0.11	0.50

SURVEILLANCE CAPSULE U AVERAGE SATURATED Co^{60} ACTIVITY

Bare Co-Al wire: $A = 1.16 \times 10^{8}$ dps/gm
Cd Shielded Co-Al wire: $A = 6.94 \times 10^{7}$ dps/gm

MONITOR FLUXES DERIVED FROM Co^{60} SATURATED ACTIVITY

$$\Phi_{2200} = 8.22 \times 10^{10} \text{ n/cm}^2\text{-sec}$$
$$\Phi_{res} = 6.00 \times 10^{10} \text{ n/cm}^2\text{-sec}$$

PRODUCT NUCLIDE LOSS RATE COMPARISON

Nuclide	Decay Constant (1/sec)	Absorption Rate $(\sigma_{2200}\,\Phi_{2200} + RI\,\Phi_{res})$ (1/sec)
Mn^{54}	2.57×10^{-8}	8.22×10^{-13}
Co^{58}	1.13×10^{-7}	5.68×10^{-10}
Co^{60}	4.17×10^{-9}	4.22×10^{-13}
Cs^{137}	7.28×10^{-10}	3.90×10^{-14}

TABLE 6-12

SUMMARY OF V. C. SUMMER FAST NEUTRON FLUENCE RESULTS

BASED UPON SURVEILLANCE CAPSULE U

Location	Current Fast ($E > 1.0$ MeV) Neutron Fluence[a] (n/cm^2)		End of Life Fast ($E > 1.0$ MeV) Neutron Fluence[b] (n/cm^2)	
	Measured[c]	Calculated	Measured[c]	Calculated
Capsule U	6.39×10^{18}	7.43×10^{18}		
Vessel IR	2.05×10^{18}	2.39×10^{18}	5.84×10^{19}	6.80×10^{19}
Vessel 1/4T	1.22×10^{18}	1.42×10^{18}	3.47×10^{19}	4.03×10^{19}
Vessel 3/4T	2.83×10^{17}	3.29×10^{17}	8.04×10^{18}	9.35×10^{18}

a) Current fluences are based on operation at 2775 MWt for 1.12 EFPY

b) EOL fluences are based on operation at 2775 MWt for 32 EFPY.

c) The measured results of surveillance Capsule U were extrapolated to the reactor vessel locations using the following calculated lead factors:

Inner Radius - 3.11
1/4 Thickness - 5.24
3/4 Thickness - 22.6

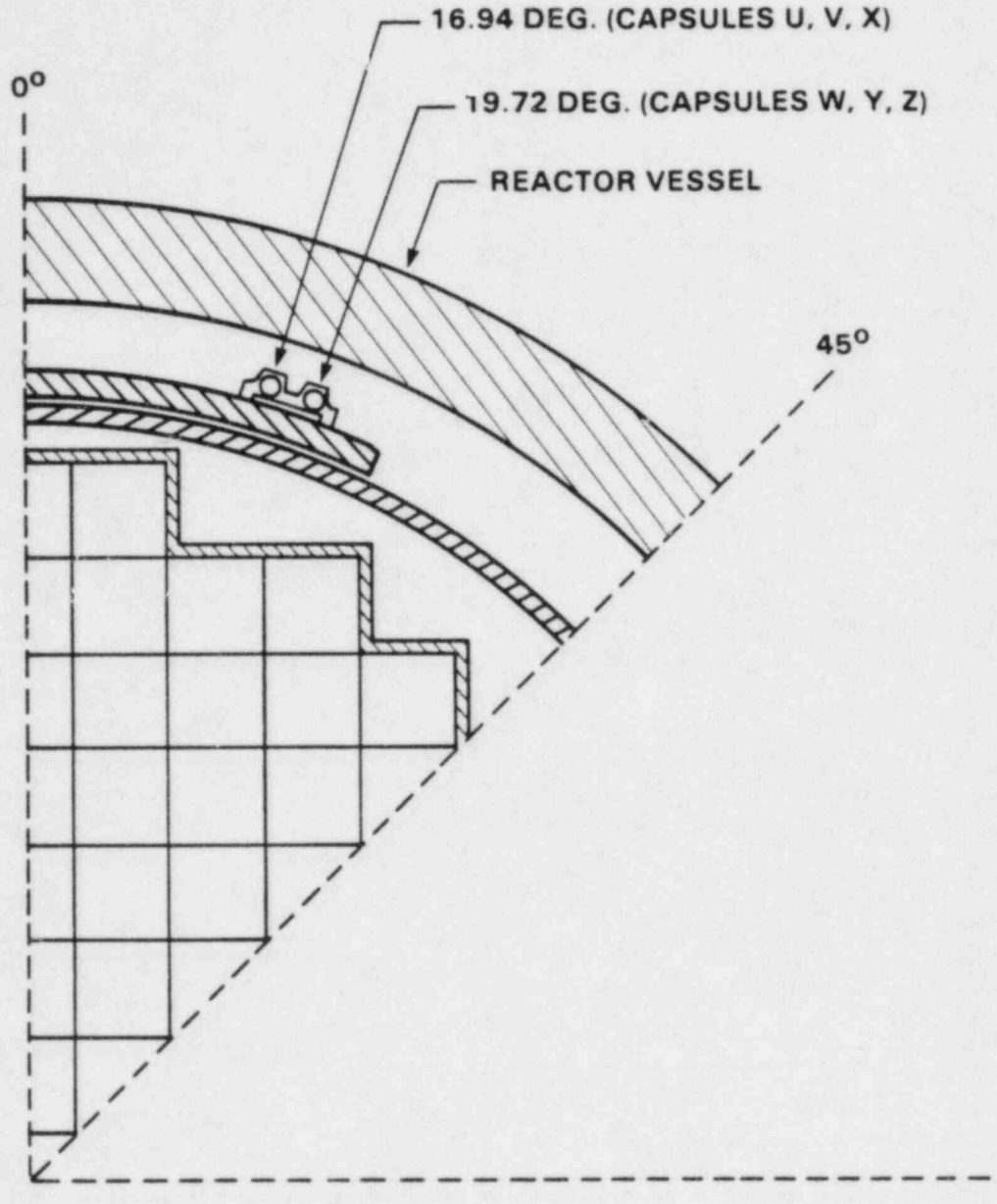

Figure 6-1. V.C. Summer Reactor Geometry

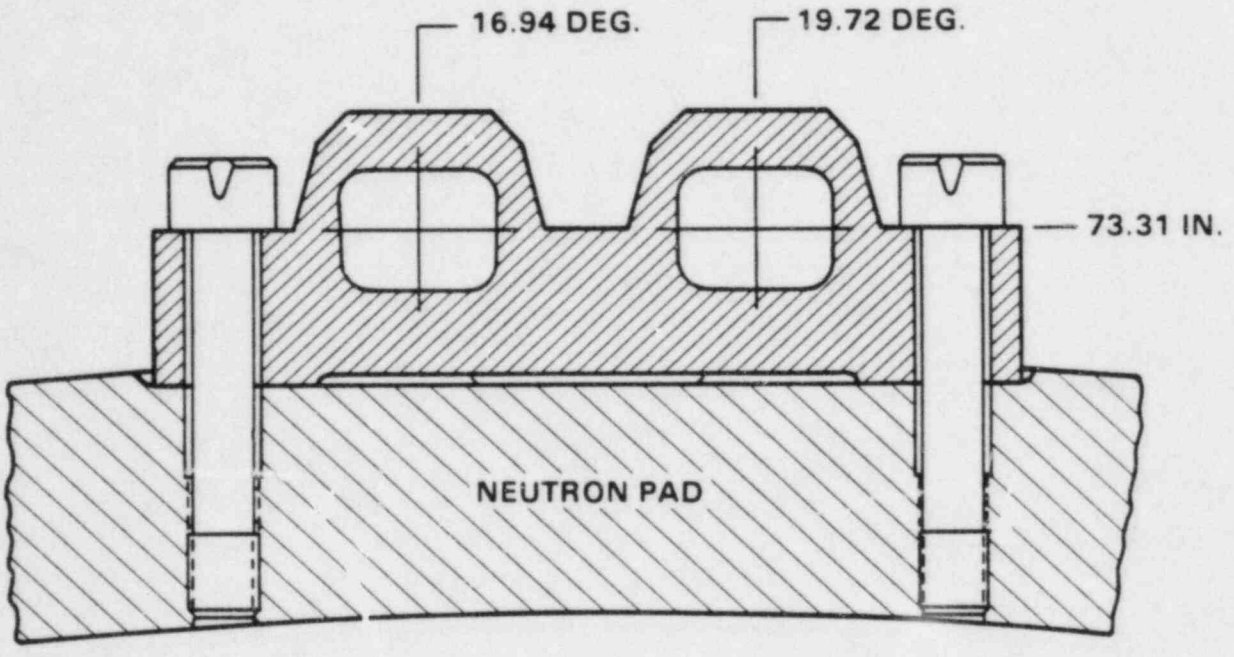

Figure 6-2. Plan View of a Dual Reactor Vessel Surveillance Capsule

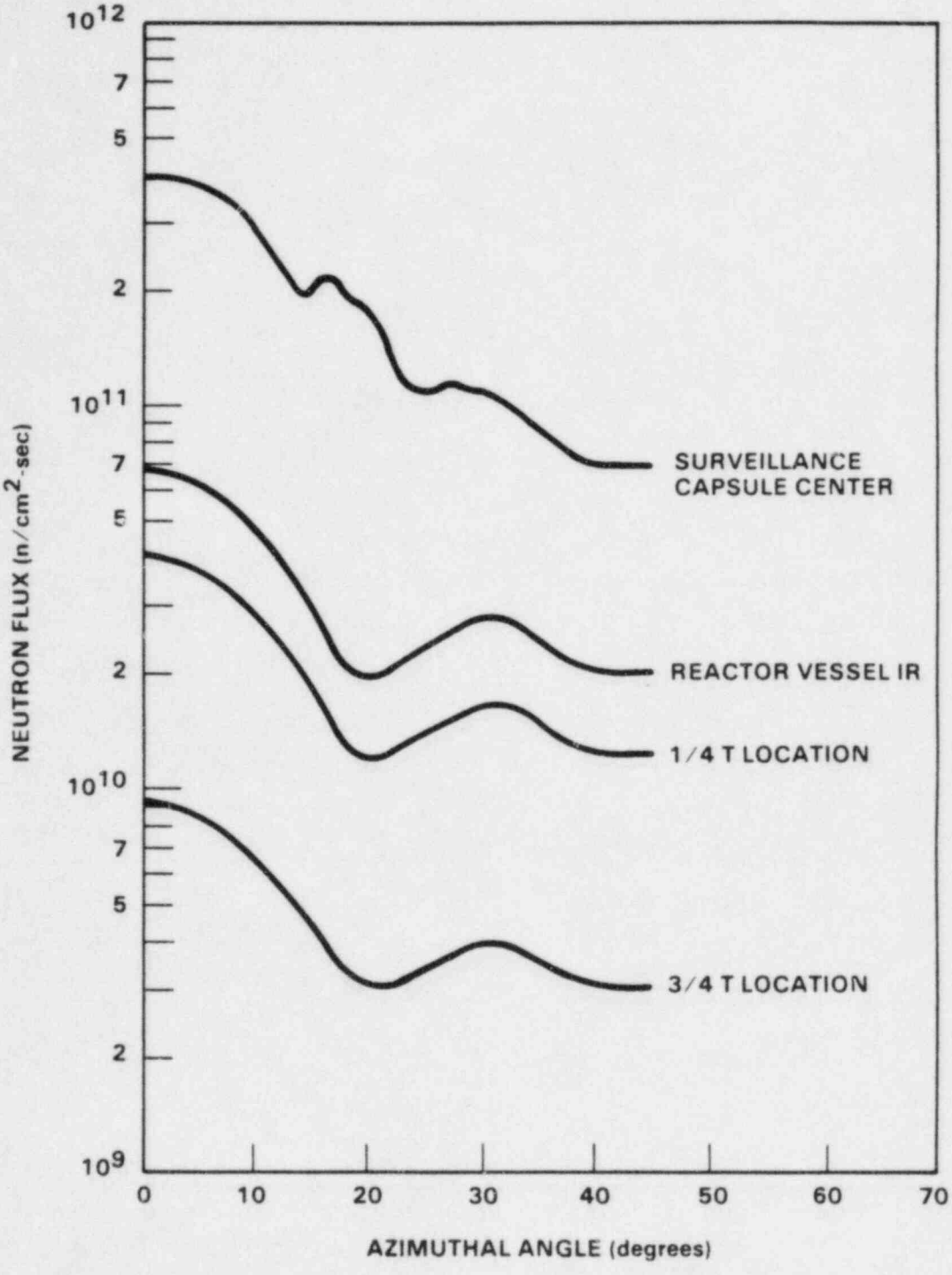

Figure 6-3. Calculated Azimuthal Distribution of Maximum Fast (E >1.0 MeV) Neutron Flux Within the Reactor Vessel — Surveillance Capsule Geometry

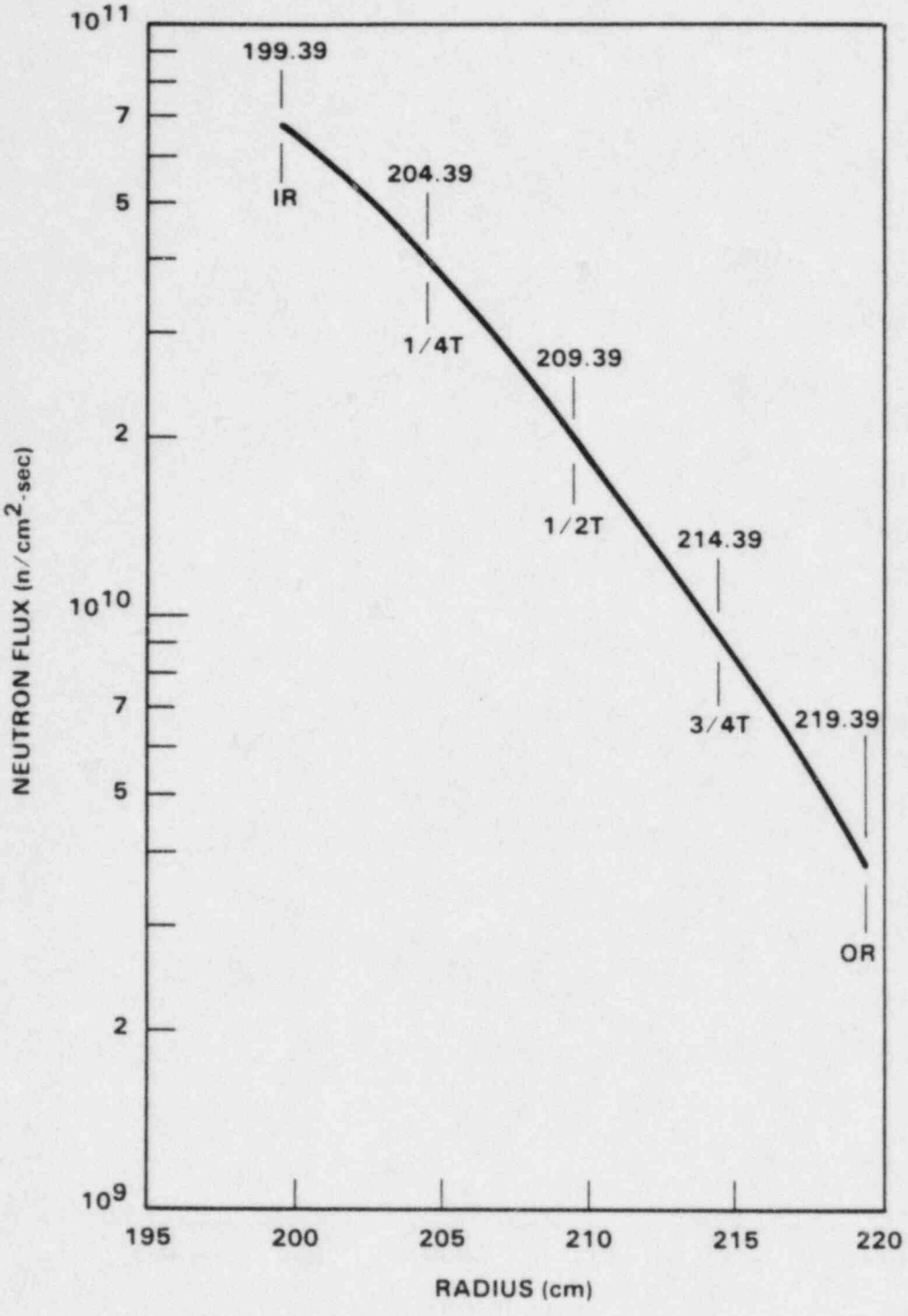

Figure 6-4. Calculated Radial Distribution of Maximum Fast (E >1.0 MeV) Neutron Flux Within the Reactor Vessel

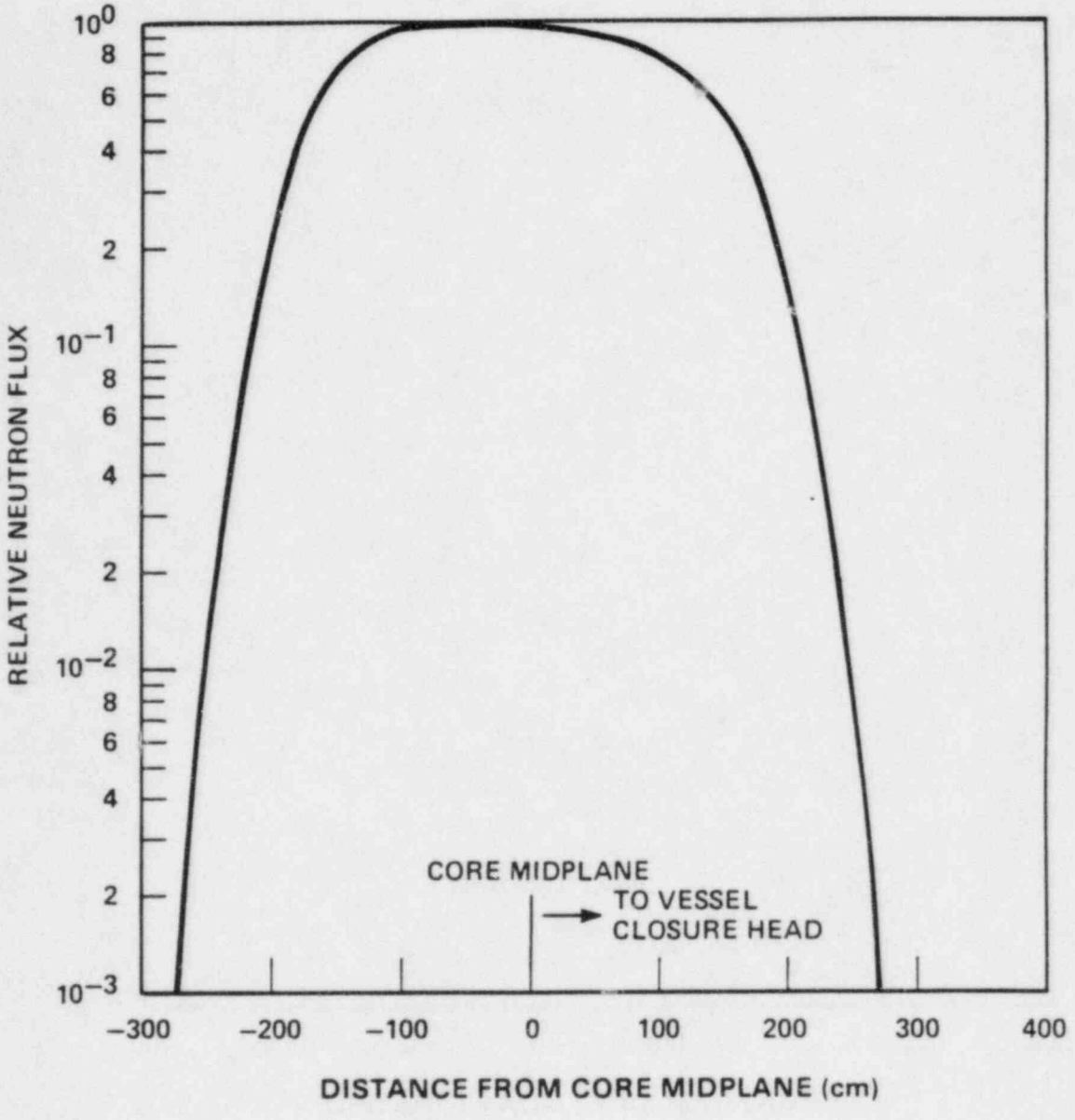

Figure 6-5. Relative Axial Variation of Fast (E > 1.0 MeV) Neutron Flux Within the Reactor Vessel

SECTION 7
SURVEILLANCE CAPSULE REMOVAL SCHEDULE

The following removal schedule meets ASTM E185-82 and is recommended for future capsules to be removed from the V. C. Summer Unit 1 reactor vessel:

Capsule	Vessel Location (deg)	Lead Factor	Removal Time[a]	Estimated Fluence (n/cm^2)
U	343°	3.11	1.12 (removed)	6.39×10^{18}
V	107°	3.11	3	1.66×10^{19}
X	287°	3.11	6	3.32×10^{19}[b]
W	110°	2.69	12	5.75×10^{19}[c]
Y	290°	2.69	20	9.58×10^{19}
Z	340°	2.69	standby	--

a. Effective full power years from plant startup
b. Approximate fluence at 1/4 thickness vessel wall at end of life
c. Approximate fluence at vessel inner wall at end of life

SECTION 8
REFERENCES

1. Davidson, J. A. and Yanichko, S. E., "South Carolina Electric and Gas Co. Virgil C. Summer Nuclear Plant Unit No. 1 Reactor Vessel Radiation Surveillance Program," WCAP-9234, January 1978.

2. ASTM E185-73 "Practive for Surveillance Tests for Nuclear Reactor" in ASTM Standards, Part 10 (1973), American Society for Testing and Materials, Philadelphia, Pa., 1973.

3. Lott, R. G. and Shogan, R. P., "V. C. Summer Unit No. 1 Nuclear Pressure Vessel Surveillance Capsule U Test Program," Westinghouse R&D Memo 85-5D2-CGEU-M1, 1985.

4. Regulatory Guide 1.99, Revision 1, "Effects of Residual Elements on Predicted Radiation Damage to Reactor Vessel Materials," U.S. Nuclear Regulatory Commission, April 1977.

5. Soltesz, R. G., Disney, R. K., Jedruch, J., and Ziegler, S. L., "Nuclear Rocket Shielding Methods, Modification, Updating and Input Data Preparation. Vol. 5 - Two-Dimensional Discrete Ordinates Transport Technique," WANL-PR(LL)-034, Vol 5, August 1970.

6. "ORNL RSIC Data Library Collection DLC-76, SAILOR Coupled Self-Shielded, 47 Neutron, 20 Gamma-Ray, P3, Cross Section Library for Light Water Reactors".

7. Benchmark Testing of Westinghouse Neutron Transport Analysis Methodology (to be published).

8. ASTM Designation E482-82, "Standard Guide for Application of Neutron Transport Methods for Reactor Vessel Surveillance," in ASTM Standards, Section 12, American Society for Testing and Materials, Philadelphia, Pa., 1984.

9. ASTM Designation E560-77, "Standard Recommended Practice for Extrapolating Reactor Vessel Surveillance Dosimetry Results," in ASTM Standards, Section 12, American Society for Testing and Materials, Philadelphia, Pa., 1984.

10. ASTM Designation E693-79, "Standard Practice for Characterizing Neutron Exposures in Ferritic Steels in Terms of Displacements per Atom (dpa)," in ASTM Standards, Section 12, American Society for Testing and Materials, Philadelphia, Pa., 1984.

11. ASTM Designation E706-81a, "Standard Master Matrix for Light-Water Reactor Pressure Vessel Surveillance Standards", in ASTM Standards, Section 12, American Society for Testing and Materials, Philadelphia, Pa., 1984.

12. ASTM Designation E853-84, "Standard Practice for Analysis and Interpretation of Light-Water Reactor Surveillance Results," in ASTM Standards, Section 12, American Society for Testing and Materials, Philadelphia, Pa., 1984.

13. ASTM Designation E261-77, "Standard Method for Determining Neutron Flux, Fluence, and Spectra by Radioactivation Techniques," in ASTM Standards, Section 12, American Society for Testing and Materials, Philadelphia, Pa., 1984.

14. ASTM Designation E262-77, "Standard Method for Measuring Thermal Neutron Flux by Radioactivation Techniques," in ASTM Standards, Section 12, American Society for Testing and Materials, Philadelphia, Pa., 1984.

15. ASTM Designation E263-82, "Standard Method for Determining Fast-Neutron Flux Density by Radioactivation of Iron," in ASTM Standards, Section 12, American Society for Testing and Materials, Philadelphia, Pa., 1984.

16. ASTM Designation E264-82, "Standard Method for Determining Fast-Neutron Flux Density by Radioactivation of Nickel," in ASTM Standards, Section 12, America Society for Testing and Materials, Philadelphia, Pa., 1984.

17. ASTM Designation E481-78, "Standard Method for Measuring Neutron-Flux Density by Radioactivation of Cobalt and Silver," in ASTM Standards, Section 12, American Society for Testing and Materials, Philadelphia, Pa., 1984.

18. ASTM Designation E523-82, "Standard Method for Determining Fast-Neutron Flux Density by Radioactivation of Copper," in ASTM Standards, Section 12, American Society for Testing and Materials, Philadelphia, Pa., 1984.

19. ASTM Designation E704-84, "Standard Method for Measuring Reaction Rates by Radioactivation of Uranium-238," in ASTM Standards, Section 12, American Society for Testing and Materials, Philadelphia, Pa., 1984.

20. ASTM Designation E705-79, "Standard Method for Measuring Fast-Neutron Flux Density by Radioactivation of Neptunium-237," in ASTM Standards, Section 12, American Society for Testing and Materials, Philadelphia, Pa., 1984.

21. ASTM Designation E1005-84, "Standard Method for Application and Analysis of Radiometric Monitors for Reactor Vessel Surveillance," in ASTM Standards, Section 12, American Society for Testing and Materials, Philadelphia, Pa., 1984.

22. Mughabghab, S. F. and Garber, D. I., "Neutron Cross-Sections," BNL-325, 3rd Edition, Volume 1, June 1973.

APPENDIX A

HEATUP AND COOLDOWN LIMIT CURVES FOR NORMAL OPERATION

A-1. INTRODUCTION

Heatup and cooldown limit curves are calculated using the most limiting value of RT_{NDT} (reference nil-ductility temperature). The most limiting RT_{NDT} of the material in the core region of the reactor vessel is determined by using the preservice reactor vessel material properties and estimating the radiation-induced ΔRT_{NDT}. RT_{NDT} is designated as the higher of either the drop weight nil-ductility transition temperature (NDTT) or the temperature at which the material exhibits at least 50 ft lb of impact energy and 35-mil lateral expansion (normal to the major working direction) minus 60°F.

RT_{NDT} increases as the material is exposed to fast-neutron radiation. Thus, to find the most limiting RT_{NDT} at any time period in the reactor's life, ΔRT_{NDT} due to the radiation exposure associated with that time period must be added to the original unirradiated RT_{NDT}. The extent of the shift in RT_{NDT} is enhanced by certain chemical elements (such as copper) present in reactor vessel steels. Design curves which show the effect of fluence and copper content on ΔRT_{NDT} for reactor vessel steels are shown in Figure A-1.

Given the copper content of the most limiting material, the radiation-induced ΔRT_{NDT} can be estimated from Figure A-1. Fast neutron fluence ($E > 1$ MeV) at the vessel inner surface, the 1/4 T (wall thickness), and 3/4 T (wall thickness) vessel locations are given as a function of full-power service life in Figure A-2. The data for all other ferritic materials in the reactor coolant pressure boundary are examined to insure that no other component will be limiting with respect to RT_{NDT}.

A-2. FRACTURE TOUGHNESS PROPERTIES

The preirradiation fracture-toughness properties of the V. C. Summer Unit 1 reactor vessel materials are presented in Table A-1. The fracture-toughness properties of the ferritic material in the reactor coolant pressure boundary are determined in accordance with the NRC Regulatory Standard Review Plan.[1] The postirradiation fracture-toughness properties of the reactor vessel beltline material were obtained directly from the V. C. Summer Unit 1 Vessel Material Surveillance Program.

A-3. CRITERIA FOR ALLOWABLE PRESSURE-TEMPERATURE RELATIONSHIPS

The ASME approach for calculating the allowable limit curves for various heatup and cooldown rates specifies that the total stress intensity factor, K_I, for the combined thermal and pressure stresses at any time during heatup or cooldown cannot be greater than the reference stress intensity factor, K_{IR}, for the metal temperature at that time. K_{IR} is obtained from the reference fracture toughness curve, defined in Appendix G of the ASME Code.[2] The K_{IR} curve is given by the equation:

$$K_{IR} = 26.78 + 1.223 \exp [0.0145 (T-RT_{NDT} + 160)] \quad (A-1)$$

where K_{IR} is the reference stress intensity factor as a function of the metal temperature T and the metal reference nil-ductility temperature RT_{NDT}. Thus, the governing equation for the heatup-cooldown analysis is defined in Appendix G of the ASME Code[2] as follows:

$$C K_{IM} + K_{It} \leq K_{IR} \quad (A-2)$$

where

K_{IM} is the stress intensity factor caused by membrane (pressure) stress

K_{It} is the stress intensity factor caused by the thermal gradients

K_{IR} is a function of temperature relative to the RT_{NDT} of the material

C = 2.0 for Level A and Level B service limits

C = 1.5 for hydrostatic and leak test conditions during which the reactor core is not critical

At any time during the heatup or cooldown transient, K_{IR} is determined by the metal temperature at the tip of the postulated flaw, the appropriate value for RT_{NDT}, and the reference fracture toughness curve. The thermal stresses resulting from temperature gradients through the vessel wall are calculated and then the corresponding (thermal) stress intensity factors, K_{It}, for the reference flaw are computed. From Equation (A-2), the pressure stress intensity factors are obtained and, from these, the allowable pressures are calculated.

For the calculation of the allowable pressure-versus-coolant temperature during cooldown, the Code reference flaw is assumed to exist at the inside of the vessel wall. During cooldown, the controlling location of the flaw is always at the inside of the wall because the thermal gradients produce tensile stresses at the inside, which increase with increasing cooldown rates. Allowable pressure-temperature relations are generated for both steady-state and finite cooldown rate situations. From these relations, composite limit curves are constructed for each cooldown rate of interest.

The use of the composite curve in the cooldown analysis is necessary because control of the cooldown procedure is based on measurement of reactor coolant temperature, whereas the limiting pressure is actually dependent on the material temperature at the tip of the assumed flaw.

During cooldown, the 1/4 T vessel location is at a higher temperature than the fluid adjacent to the vessel ID. This condition, of course, is not true for the steady-state situation. It follows that, at any given reactor coolant temperature, the ΔT developed during cooldown results in a higher value of K_{IR} at the 1/4 T location for finite cooldown rates than for steady-state

operation. Furthermore, if conditions exist such that the increase in K_{IR} exceeds K_{It}, the calculated allowable pressure during cooldown will be greater than the steady-state value.

The above procedures are needed because there is no direct control on temperature at the 1/4 T location and, therefore, allowable pressures may unknowingly be violated if the rate of cooling is decreased at various intervals along a cooldown ramp. The use of the composite curve eliminates this problem and insures conservative operation of the system for the entire cooldown period.

Three separate calculations are required to determine the limit curves for finite heatup rates. As is done in the cooldown analysis, allowable pressure-temperature relationships are developed for steady-state conditions as well as finite heatup rate conditions assuming the presence of a 1/4 T defect at the inside of the vessel wall. The thermal gradients during heatup produce compressive stresses at the inside of the wall that alleviate the tensile stresses produced by internal pressure. The metal temperature at the crack tip lags the coolant temperature; therefore, the K_{IR} for the 1/4 T crack during heatup is lower than the K_{IR} for the 1/4 T crack during steady-state conditions at the same coolant temperature. During heatup, especially at the end of the transient, conditions may exist such that the effects of compressive thermal stresses and lower K_{IR}'s do not offset each other, and the pressure-temperature curve based on steady-state conditions no longer represents a lower bound of all similar curves for finite heatup rates when the 1/4 T flaw is considered. Therefore, both cases have to be analyzed in order to insure that at any coolant temperature the lower value of the allowable pressure calculated for steady-state and finite heatup rates is obtained.

The second portion of the heatup analysis concerns the calculation of pressure-temperature limitations for the case in which a 1/4 T deep outside surface flaw is assumed. Unlike the situation at the vessel inside surface, the thermal gradients established at the outside surface during heatup produce stresses which are tensile in nature and thus tend to reinforce any pressure stresses present. These thermal stresses are dependent on both the rate of

heatup and the time (or coolant temperature) along the heatup ramp. Since the thermal stresses at the outside are tensile and increase with increasing heatup rates, each heatup rate must be analyzed on an individual basis.

Following the generation of pressure-temperature curves for both the steady-state and finite heatup rate situations, the final limit curves are produced by constructing a composite curve based on a point-by-point comparison of the steady-state and finite heatup rate data. At any given temperature, the allowable pressure is taken to be the lesser of the three values taken from the curves under consideration. The use of the composite curve is necessary to set conservative heatup limitations because it is possible for conditions to exist wherein, over the course of the heatup ramp, the controlling condition switches from the inside to the outside and the pressure limit must at all times be based on analysis of the most critical criterion.

Finally, the new 10CFR50[3] rule which addresses the metal temperature of the closure head flange and vessel flange regions is considered. This 10CFR50 rule states that the metal temperature of the closure flange regions must exceed the material RT_{NDT} by at least 120°F for normal operation when the pressure exceeds 20 percent of the preservice hydrostatic test pressure (621 psig for V. C. Summer Unit 1). Table A-1 indicates that the limiting RT_{NDT} of 10°F occurs in the head flange of V. C. Summer Unit 1, and the minimum allowable temperature of this region is 130°F at pressures greater than 621 psig.

A-4. HEATUP AND COOLDOWN LIMIT CURVES

Limit curves for normal heatup and cooldown of the primary Reactor Coolant System have been calculated using the methods discussed in Section A-3. The derivation of the limit curves is presented in the NRC Regulatory Standard Review Plan.[4]

Transition temperature shifts occurring in the pressure vessel materials due to radiation exposure have been obtained directly from the reactor pressure vessel surveillance program. Charpy test specimens from Capsule U indicate that both the surveillance weld metal and core region intermediate shell plate code no. A9154-1 exhibited shifts in RT_{NDT} of 30°F at a fluence of 6.39 x 10^{18} n/cm^2. This shift is well within the appropriate design curve (Figure A-1) prediction. Therefore, the heatup and cooldown curves in Figures A-3 and A-4 are based on the trend curve in Figure A-1, and these curves are applicable up to 8 effective full power years (EFPY). The heatup curve in Figure A-3 is not impacted by the new 10CFR50 rule. However, the cooldown curve in Figure A-4 is impacted by this 10CFR50 rule.

If the Regulatory Guide 1.99 Revision 1 trend curve were to be used, the heatup and cooldown curves would then be applicable up to 11 EPPY. However, the trend curve in Figure A-1 is more realistic. As a result, the 8 EFPY curves in Figures A-3 and A-4 are recommended for normal operation.

Allowable combinations of temperature and pressure for specific temperature change rates are below and to the right of the limit lines shown on the heatup and cooldown curves. The reactor must not be made critical until pressure-temperature combinations are to the right of the criticality limit line shown in Figure A-3. This is in addition to other criteria which must be met before the reactor is made critical.

The leak test limit curve shown in Figure A-3 represents minimum temperature requirements at the leak test pressure specified by applicable codes. The leak test limit curve was determined by methods of References 2 and 4.

Figures A-3 and A-4 define limits for insuring prevention of nonductile failure.

TABLE A-1 REACTOR VESSEL TOUGHNESS DATA (UNIRRADIATED)

Component	Heat No.	Grade	Cu %	P %	Ni %	NDT °F	50 Ft-Lb 35 Mil Temp °F	RT_{NDT} °F	MWD[a] Shelf Energy Ft-lbs	NMWD[b] Shelf Energy Ft-lbs
Closure Dome	A9231-1	A533B CL. 1	-	.009	.46	-20	40	-20	-	106.0
Head Flange 1	5297-V1	A508 CL. 2	-	.009	.70	10	<60	10	-	129.0
Vessel Flange	5301-V1	" "	-	.007	.70	0	<60	0	-	172.0
Inlet Nozzle	436B-1	" "	-	.005	.76	-20	<40	-20	-	130.0
" "	436B-2	" "	-	.005	.81	0	<60	0	-	114.5
" "	436B-3	" "	-	.005	.81	-20	<40	-20	-	135.0
Outlet Nozzle	437B-1	" "	-	.007	.81	-10	<50	-10	-	146.0
" "	437B-2	" "	-	.006	.80	-10	<50	-10	-	165.0
" "	437B-3	" "	-	.006	.78	0	<50	0	-	150.0
Nozzle Shell	C9955-2	A533B CL. 1	.13	.010	.57	-20	78	18	-	100.5
" "	C0123-2	" "	.12	.009	.58	-30	86	26	-	91.0
Inter. Shell	A9154-1	" "	.10	.009	.51	-20	90	30	136	80.5
" "	A9153-2	" "	.09	.006	.45	-20	40	-20	141	106.5
Lower Shell	C9923-2	" "	.08	.005	.41	-10	70	10	161	91.5
" "	C9923-1	" "	.08	.005	.41	-30	70	10	148	106.0
Bottom Hd. Ring	A9249-1	" "	-	.010	.53	-40	23	-37	-	107.0
Bottom Dome	A9231-2	" "	-	.010	.45	-10	42	-10	-	134.0
Inter. to Lower Shell Girth Weld			.06	.013	.89	-50	16	-44	-	84.0
Inter. & Lower Shell Long. Welds			.06	.013	.89	-50	16	-44	-	84.0
Weld HAZ			-	-	-	-70	-37	-70	-	130.0

(a) Major Working Direction

(b) Normal to Major Working Direction

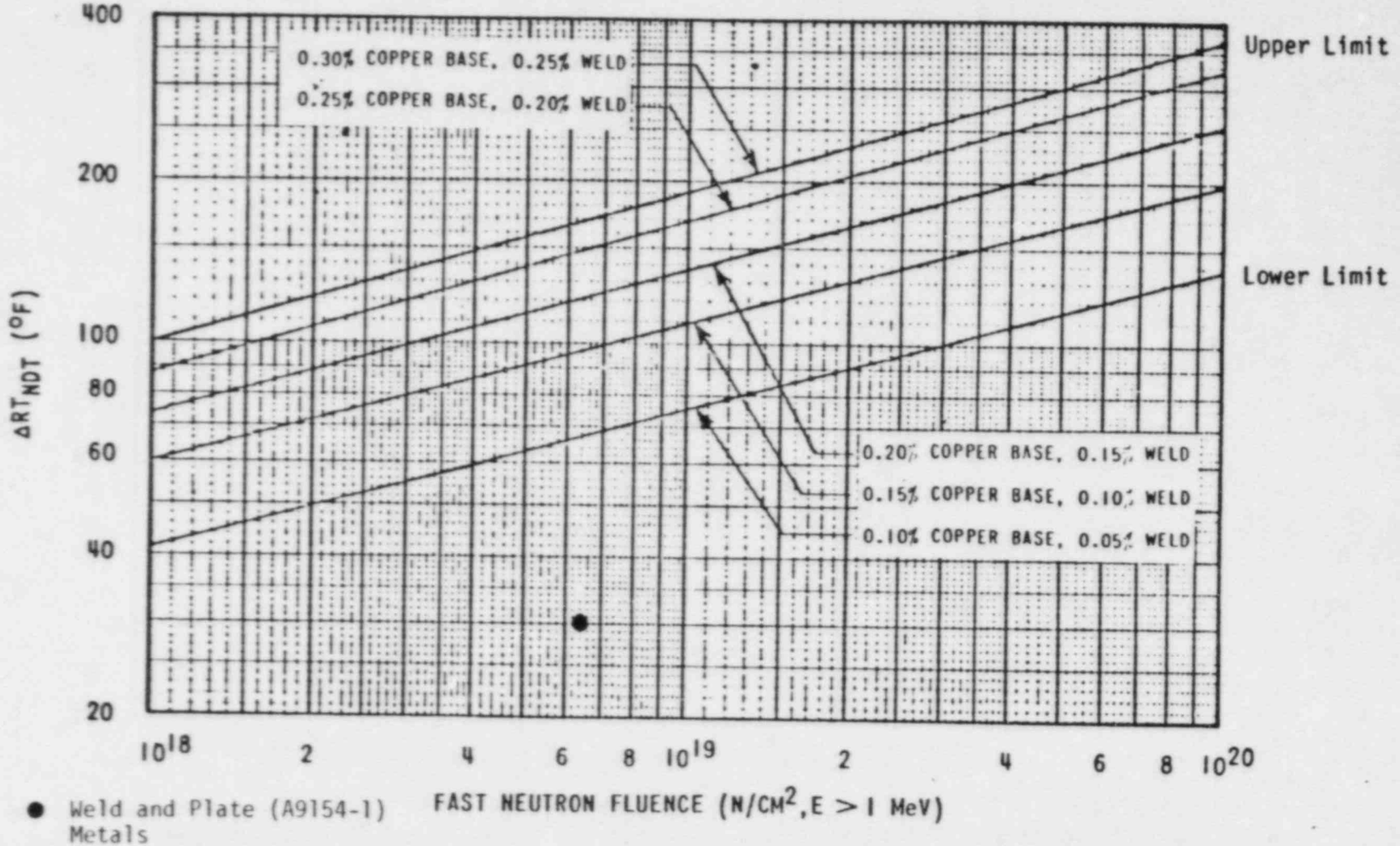

FIGURE A-1 Effect of Fluence and Copper on Shift of RT_{NDT} for Reactor Vessel Steels Exposed to Irradiation at 550°F

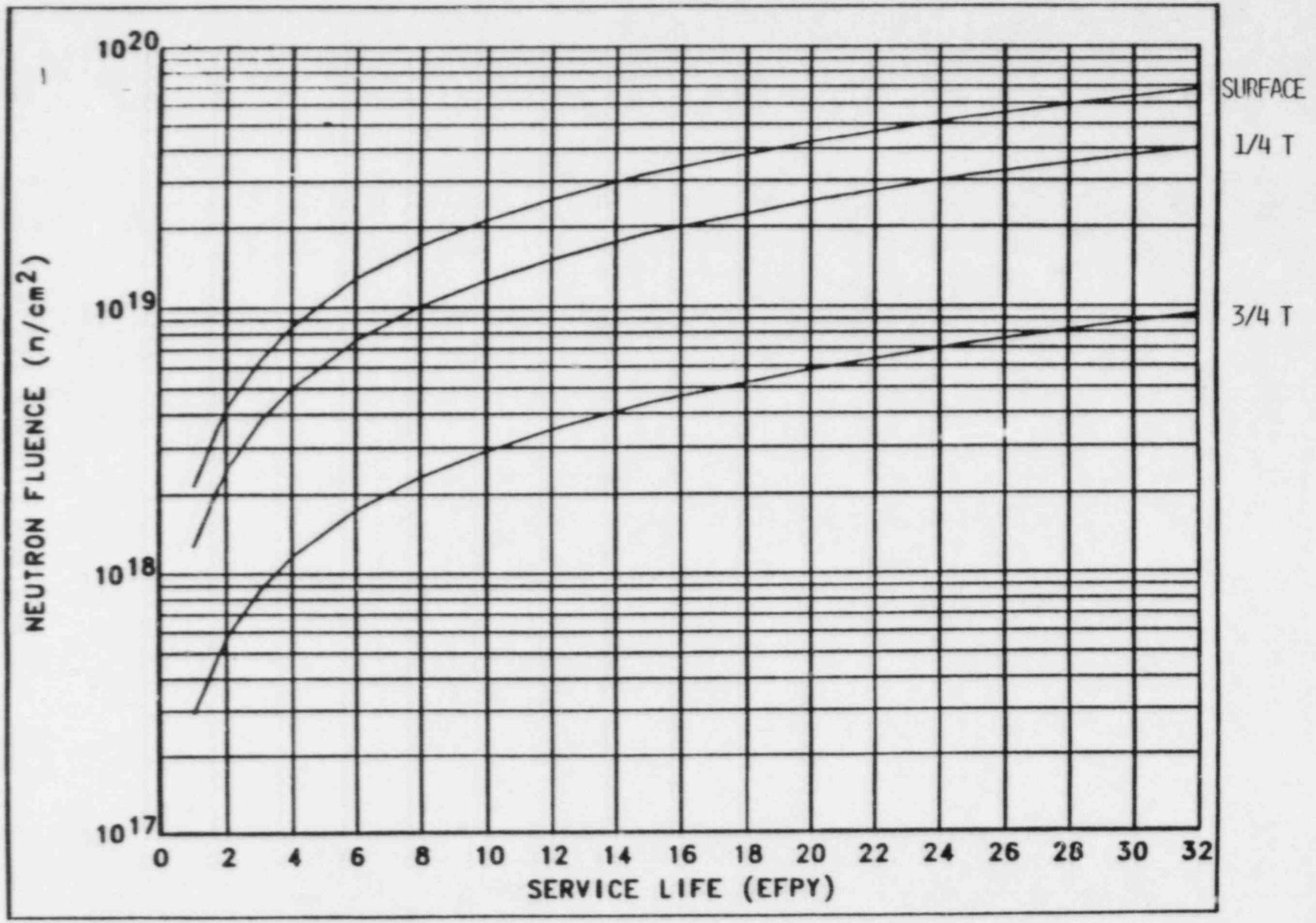

FIGURE A-2. FAST NEUTRON FLUENCE (E>1 MEV) AS A FUNCTION OF FULL POWER SERVICE LIFE (EFPY)

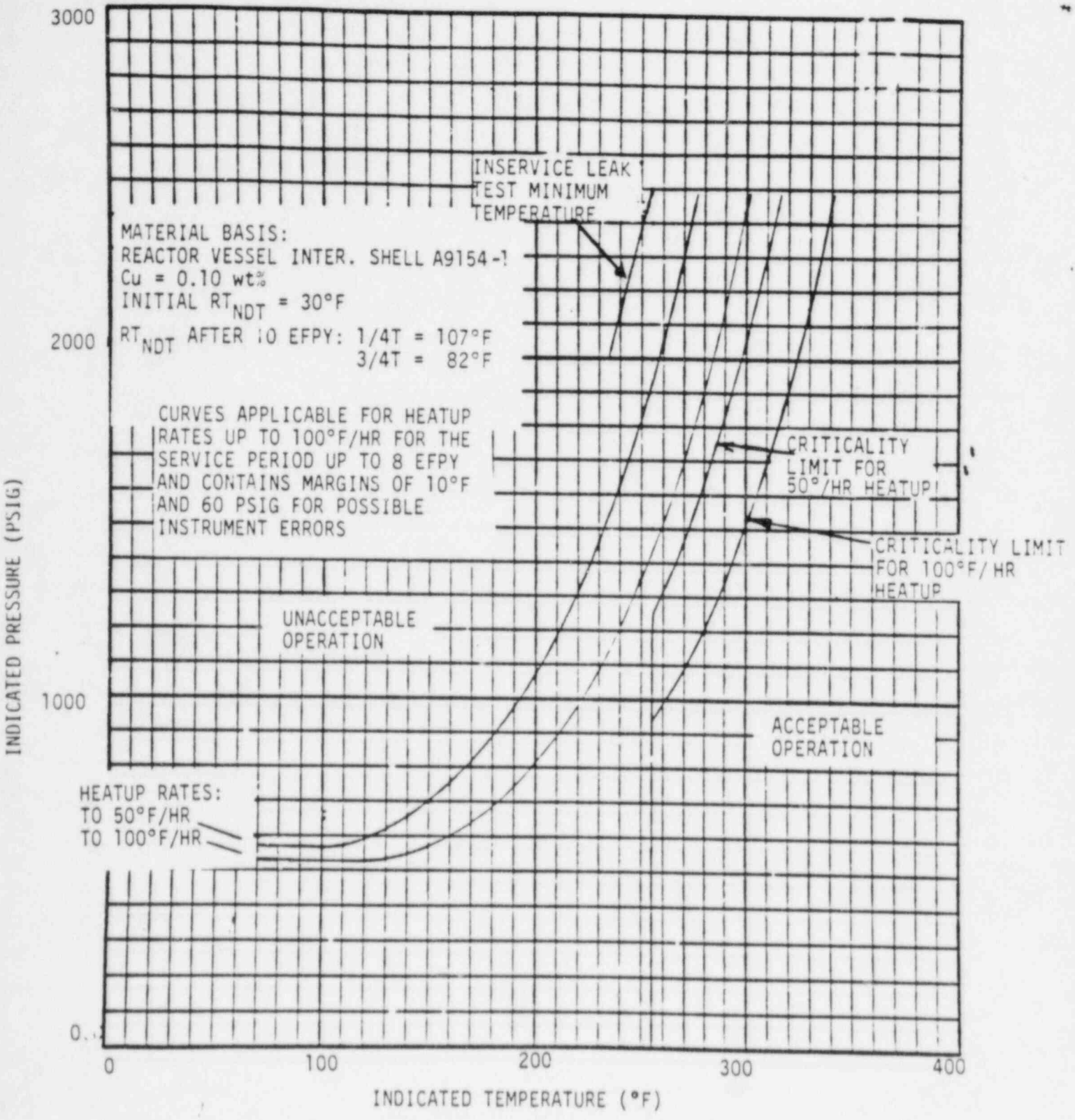

FIGURE A-3 Virgil C. Summer Unit 1 Reactor Coolant System Heatup Limitations Applicable up to 8 EFPY

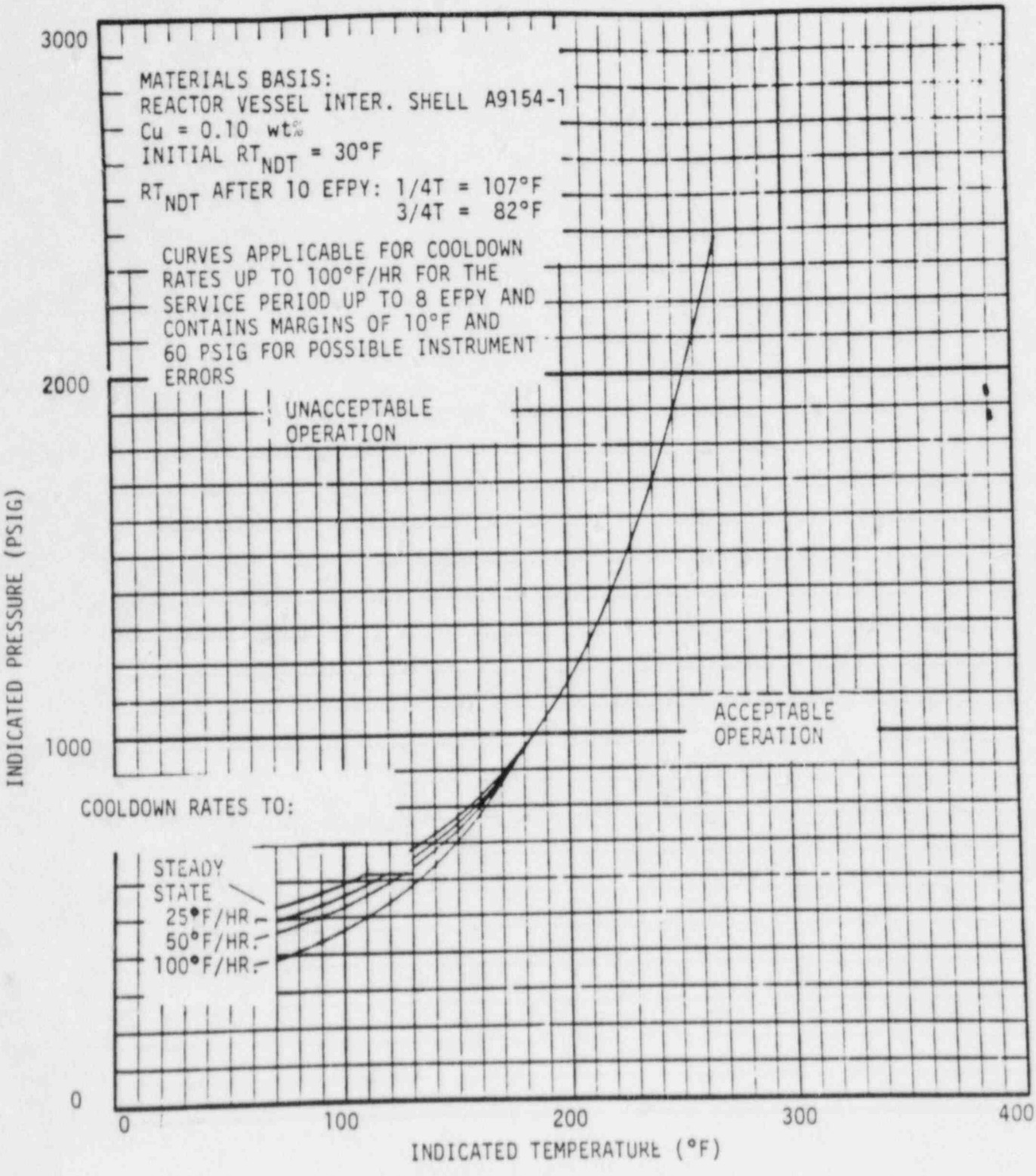

FIGURE A-4 Virgil C. Summer Unit 1 Reactor Coolant System Cooldown Limitations Applicable up to 8 EFPY

APPENDIX A

REFERENCES

1. "Fracture Toughness Requirements," Branch Technical Position MTEB 5-2, Chapter 5.3.2 in Standard Review Plan for the Review of Safety Analysis Reports for Nuclear Power Plants, LWR Edition, NUREG-0800, 1981.

2. ASME Boiler and Pressure Vessel Code, Section III, Division 1 - Appendices, "Rules for Construction of Nuclear Vessels," Appendix G, "Protection Against Nonductile Failure," pp. 559-564, 1983 Edition, American Society of Mechanical Engineers, New York, 1983.

3. Code of Federal Regulations, 10CFR50, Appendix G, "Fracture Toughness Requirements," U.S. Nuclear Regulatory Commission, Washington, D.C., Amended May 17, 1983 (48 Federal Register 24010).

4. "Pressure-Temperature Limits," Chapter 5.3.2 in Standard Review Plan for the Review of Safety Analysis Reports for Nuclear Power Plants, LWR Edition, NUREG-0800, 1981.